LITHOS 472-473 (2024) 107575

Contents lists available at ScienceDirect

LITHOS

journal homepage: www.elsevier.com/locate/lithos

Mineralogical and petrological constraints and tectonic implications of a new coesite-bearing unit from the Alpine Tethys oceanic slab (Susa Valley, Western Alps)

Stefano Ghignone [a,*], Mattia Gilio [b,c], Alessia Borghini [d,e], Federica Boero [a], Marco Bruno [a,f], Emanuele Scaramuzzo [g]

[a] Earth Sciences Department, University of Turin, Via Valperga Caluso 35, 10125 Torino, Italy
[b] Earth and Environmental Sciences Department, University of Pavia, via Ferrata 1, 27100 Pavia, Italy
[c] Erdsystemwissenschaften, Universität Hamburg, Grindelallee 48, D-20146 Hamburg, Germany
[d] Faculty of Geology, Geophysics and Environmental Protection, AGH University of Science and Technology, Aleja Mickiewicza 30, 30-059 Krakow, Poland
[e] Institut für Geowissenschaften, Universität Potsdam, Karl-Liebknecht-Straße 24/25, 14476 Potsdam-Golm, Germany
[f] NIS, Center for Nanostructured Interfaces and Surfaces, Università degli Studi di Torino, Via G. Quarello 15/a, 10135 Torino, Italy
[g] Department of Science and High Technology, University of Insubria, via Valleggio 11, 22100 Como, Italy

ARTICLE INFO

Keywords:
Coesite
UHP
Garnet
Elastic geobarometry
Western Alps

ABSTRACT

Worldwide, Ultrahigh Pressure (UHP) oceanic units are rare and to date only three were recognized: Tianshan (China), and Lago di Cignana and Lago Superiore Unit (Western Alps, Italy). The UHP oceanic units represent the only geological object directly exhumed from mantle depth and they record fundamental information about processes occurring in the deepest portions of the subduction interface.

In this work, we describe the occurrence of a new UHP oceanic unit within the Western Alps (mid Susa Valley, Internal Piedmont Zone). We here report the finding of a UHP index mineral, i.e., coesite and we provide a detailed study of garnet inclusions in metapelites and metabasites part of the meta-sedimentary cover of the meta-ophiolites cropping out in the mid Susa Valley. The samples were investigated via optical microscope, Raman spectroscopy, Elastic Geothermometry and classic thermometry (Zr-in-rutile) in order to constrain the P-T evolution of the area.

The finding of a new UHP unit in the Internal Piedmont Zone, together with the already described Lago di Cignana and Lago Superiore units, points towards the possible existence of a UHP oceanic slice that reached a similar peak-P (i.e., the return point) along the same subduction gradient. This slice was then removed from the slab and dismembered during exhumation, and it is now exposed as coesite-bearing units juxtaposed with lower pressure eclogite-facies ophiolites. Moreover, the large occurrence of coesite along the entire Internal Piedmont Zone significantly increases the extension of the UHP oceanic units. Hence, the model of a localized non-lithostatic pressure is at the state of the art difficult to apply to the oceanic units of the Western Alps.

1. Introduction

The occurrence of UHP index minerals (i.e., coesite, microdiamond, majorite, moissanite overall, Chopin, 1984; Smith, 1984; Sobolev and Shatsky, 1990; Chopin, 2003; von Roermund et al., 2002) in tectono-metamorphic belts is of paramount importance to attest the depths attained during subduction of the continental and oceanic lithosphere (e.g., Kylander-Clark et al., 2012). In the four decades after the first findings of coesite in the Alps (Chopin, 1984) and Caledonides (Smith, 1984), UHP minerals have been increasingly found in orogens of different age and location for a total of ~30 (see Gilotti, 2013 and references therein). Nevertheless, between these UHP units only three are made by oceanic lithosphere: (1) Western Tianshan (China; Zhang et al., 2002), (2) Lago di Cignana Unit (Reinecke, 1991) and (3) Monviso, Lago Superiore Unit (Ghignone et al., 2023a); Lago di Cignana Unit and Lago Superiore Unit are both in the Internal Piedmont Zone of the Western Italian Alps (Fig. 1a; IPZ, Bearth, 1967; Dal Piaz et al., 2003).

Meta-ophiolitic sutures represent the only direct access to a paleo-

* Corresponding author.
E-mail address: s.ghignone@unito.it (S. Ghignone).

https://doi.org/10.1016/j.lithos.2024.107575
Received 21 December 2023; Received in revised form 5 March 2024; Accepted 7 March 2024
Available online 15 March 2024

subduction slab otherwise inaccessible. The studies of this geological object open a window into the deepest processes occurring inside a subduction zone. In this context, the Alpine meta-ophiolitic suture constitute a perfect case study as it is entirely preserved from Genova to Vienna. Coesite-bearing meta-ophiolites (Ghignone et al., 2023a; Reinecke, 1991) in the Western Alps yield the extraordinary opportunity to study deep processes of a plate interface (Agard, 2021). As stated above, UHP oceanic units are extremely rare: their formation and actual position in the Western Alps was explained by the following models: (i) lithostatic re-equilibration under regional-scale at roughly constant metamorphic conditions (see e.g., Agard, 2021 and references therein), (ii) mixing of different exotic blocks in a subduction channel (sensu Cloos and Shreve, 1988) (iii) localized non-lithostatic tectonic pressure (i.e., overpressure; Mancktelow, 1993; Tajčmanová et al., 2021).

Although the interpretation of the Internal Piedmont Zone as a stack of coherent oceanic lithosphere slices is generally accepted (e.g., Angiboust et al., 2009; Ghignone et al., 2021a; Agard, 2021;), the direct evidence of a coherent UHP zone is still missing. However, isolated UHP units such as the Lago di Cignana Unit, were often interpreted as the result of local non-lithostatic pressure variation, i.e., overpressure (Tajčmanová et al., 2021) due to their narrow lens-like shape, their limited size and the sharp pressure gap with surrounding units (Compagnoni and Rolfo, 2003). Nevertheless, the homogeneity of the gradient (T/P) among different localities suggests an orogen-scale mostly lithostatic pressure and excludes overpressure (Agard, 2021).

Here we report the occurrence of coesite in the mid Susa Valley, Internal Piedmont Zone (Western Alps, Italy). In this area, micrometric coesite inclusions in garnet have been detected via μ-Raman spectroscopy; characterization of the coesite inclusions together with a detailed garnet inclusions study was performed to connect the stable mineral assemblage with each stage of garnet growth. Elastic geothermobarometry (quartz in garnet and zircon in garnet) and Zr-in-rutile geothermometry helped to constrain the peak-P metamorphic conditions and the P-T path recorded by these rocks. The results were compared with P-T estimates obtained with thermodynamic modelling (Ghignone et al., 2021a) and with the other two UHP oceanic units. Our new coesite finding in the Susa Valley points out that the former Alpine Tethys oceanic slab reached a similar depth along the same gradient. This suggests that a larger volume (respect to what was previously thought) of oceanic lithosphere was subducted at >100 km depth. UHP metamorphism was not localized to limited rock volumes as the result of tectonic overpressures; rather, the fossil Alpine plate interface was likely subject to orogeny-scale lithostatic pressure.

2. Geological framework and Piedmont Zone outlines

The Western Alps (Fig. 1a) consist of continental- and oceanic-derived units subducted to HP-UHP metamorphic conditions during the Alpine subduction event (Bousquet et al., 2008; Schmid et al., 2017). The most deformed units (oceanic and continental) together with those recording the higher peak equilibration pressure occur along the axial sector of the Alpine chain (e.g., Beltrando et al., 2010). The oceanic units

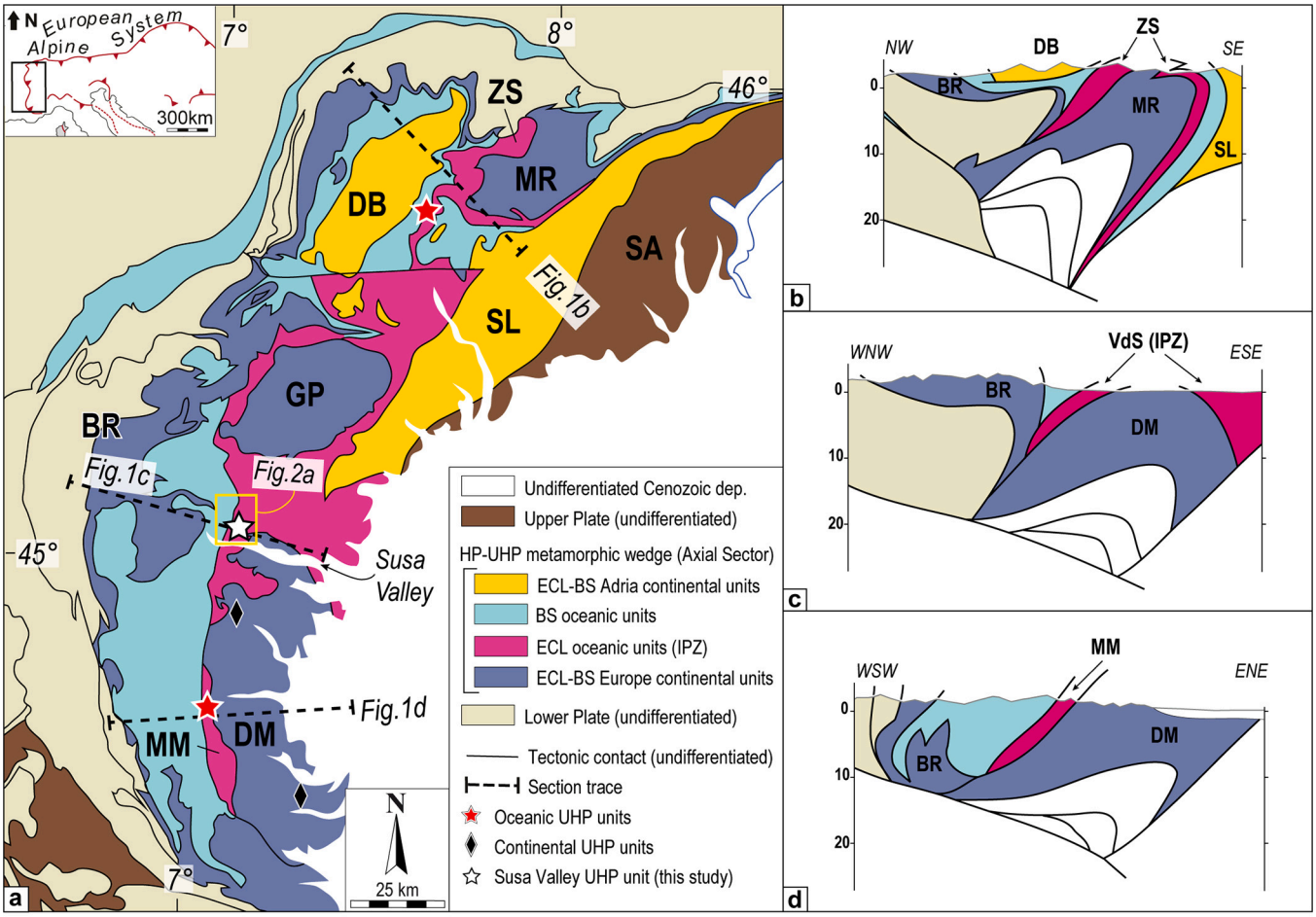

Fig. 1. a) Simplified structural and metamorphic map of the Western Alps. Codes: BR = Briançonnais; DB = Dent Blanche; DM = Dora Maira; GP = Gran Paradiso; MM = Monviso Massif; MR = Monte Rosa; SA = Southern Alps; SL = Sesia-Lanzo; ZS = Zermatt-Saas, modified after Ballèvre et al. (2020); Ghignone et al. (2023a); De Togni et al. (2023). Interpreted crustal-scale sections in correspondence of the UHP meta-ophiolite units: b) Lago di Cignana Unit, c) Susa Valley, d) Lago Superiore Unit, modified after Schmid et al. (2017); Ballèvre et al. (2020).

represent subducted portions of the former Tethyan ocean (the so-called Piedmont Zone, Bearth, 1967) and crop out along the entire axial sector structurally above the eclogite-facies Europe-derived continental units (i.e., Dora Maira, Gran Paradiso, Monte Rosa; see e.g., Dal Piaz et al., 2003).

The Western Alps contain several UHP units of both continental and oceanic affinity. Those deriving from the European continental crust are the Brossasco-Isasca (Chopin, 1984; Xiong et al., 2021) and Chasteiran Units (Manzotti et al., 2022) of the Dora Maira Massif; the ones of oceanic affinity are the Lago di Cignana and the Lago Superiore Units (Reinecke, 1991; Ghignone et al., 2023a, respectively).

The Piedmont Zone is classically divided in two subunits according to their different structural position, lithostratigraphy, deformation style and peak metamorphic conditions: (1) the blueschist-facies External Piedmont Zone (EPZ) above and the (2) eclogite-facies Internal Piedmont Zone (IPZ) below (Bearth, 1967). The External Piedmont Zone (i.e., the Schistes Lustrés) records metamorphic peak in blueschist-facies conditions (e.g., Agard et al., 2001) and consists of a thick sequence of metasediments with embedded meta-ophiolite bodies. Differently, the Internal Piedmont Zone consists of meta-ophiolites (serpentinite, metagabbro, metabasalt) with a thin metasedimentary cover (mainly calcschist and minor marble, micaschist, quartzite; Ghignone et al., 2020a; De Togni et al., 2021 and references therein), re-equilibrated at (U)HP conditions and then overprinted in greenschist facies (see e.g., Bucher et al., 2005; Groppo et al., 2009, 2019).

The peak P-T conditions estimated on the meta-ophiolites in the different sectors of the Internal Piedmont Zone yield roughly similar results. In the northern meta-ophiolites (i.e., the Zermatt-Saas Unit) were estimated $P = 2.6–2.8$ GPa and $T = 540–600$ °C (Angiboust et al., 2009; Bucher et al., 2005; Groppo et al., 2009). In the southern meta-ophiolites (i.e., the Monviso Massif) were obtained instead P = 2.6–2.9 GPa and $T = 530–550$ °C (Angiboust et al., 2012; Gilio et al., 2020).

The Internal Piedmont Zone also hosts the UHP Lago di Cignana (Fig. 1b; LCU, $P = 3.0–3.2$ GPa, $T = 590–600$ °C; Reinecke, 1991; Groppo et al., 2009; Frezzotti et al., 2011) and Lago Superiore Units (Fig. 1d; LSU, $P = 2.8–2.9$ GPa, $T = 500–520$ °C; Ghignone et al., 2023a) in the south.

The Susa Valley Unit, studied here, also belongs to the eclogitic Internal Piedmont Zone of the Western Alps (Figs. 1c, 2a) and crop out in the same structural position as the UHP oceanic units described above (Fig. 1a, b, d). It is sandwiched between the blueschist-facies meta-ophiolites of the External Piedmont Zone and the Dora-Maira underneath (Gasco et al., 2011; Ghignone et al., 2020b and references therein) and is bounded to the E by a splay of the Insubric lineament (Lis-Trana deformation Zone, Balestro et al., 2009) and to the W by the Susa Shear Zone (SSZ), a first-order shear zone responsible for the coupling between the Internal and the External Piedmont Zones (Ghignone et al., 2020a, 2020b).

The Susa Valley is constituted by serpentinites and a few metagabbro bodies, overlain by metabasalts and metasedimentary rocks, mainly calcschist, garnet-micaschist, quartzite and impure marble (Ghignone et al., 2020a, 2020b). Alpine P-T metamorphic conditions of the Internal Piedmont Zone in this area were estimated to be $P = 2.5–2.9$ GPa, $T = 460–510$ °C, consistent with the possible occurrence of coesite (Ghignone et al., 2021a).

3. Materials and methods

3.1. Mineral analysis

We used a microprobe JEOL JXA-8200 available at the University of Potsdam. The instrument is equipped with five wavelength dispersive spectrometers (WDS) to determine garnet major element composition and the concentration of Zr in rutile. Garnets were analyzed with an acceleration voltage of 15 kV, a current of 15 nA and a beam diameter of 2 μm whereas garnets maps were performed with the same acceleration voltage but higher current (35 nA) and smaller beam diameter (1 μm). Due to the small size of the grains the analyses of Zr concentration in rutile were possible to perform only for one sample, VS15. The instrument was set with an acceleration voltage of 20 kV, a current of 100 nA and a beam diameter of 2 μm. The microprobe was calibrated using the rutile standard 61,568 from the University of Heidelberg that was also measured before and after the set of analyses on the sample. The detection limit determined for the analyses is 10 ppm of Zr and all the measurement ≤10 ppm were excluded.

Representative WDS analyses of garnet are reported in Table S1.

3.2. Raman analysis

We measured the Raman spectra of coesite, quartz and zircon inclusions in garnet with a HORIBA instrument, coupled with a Jobin Yvon HR800 spectrometer and a CCD detector (holographic gratings of 1800 grooves/mm) equipped with an Olympus BX41 confocal microscope at controlled temperature of 20(±1) °C, at the University of Turin, Dept. of Earth Sciences. Raman spectra were excited using the 532 nm line of a solid state (YAG) laser. The spectrometer was calibrated to the Raman peak of silicon at 520.6 cm^{-1}. We used spectra of free crystals with the same composition as the inclusions as further calibration for the entire spectral range used in our investigation. The collected spectra were baseline-corrected for the continuum luminescence background, when necessary, temperature-reduced to account for the Bose-Einstein occupation factor and normalized to the acquisition time. Peak positions, full widths at half maximum (FWHMs), and integrated intensities were determined from fits with pseudo-Voigt functions. To reduce strain interference due to inclusion proximity to the sample surface, we prepared a section 120 μm-thick, and we only analyzed non-faceted, rounded and sub-rounded inclusions, isolated up to three times their radius, following the approach developed by Mazzucchelli et al. (2018) and Campomenosi et al. (2018). For each of the selected Raman bands we determined the shift ($\Delta\omega$) of the Raman band as the difference between the Raman shift of the inclusion (ω_i) from that of an unstrained reference crystal (ω_0). As standards, we used free (unstrained) quartz and zircon (Mud Tank Hill, Australia) crystals, measured multiple times during each measurement session at ambient pressure and room temperature (0.1 MPa and 20 °C) to eliminate shifts in peak positions due to instrumental drift and/or minor changes in room temperature. The ω0 values were averaged and then subtracted from the ωi of the strained inclusions analyzed in between two consecutive standard measurements. For zircon inclusions, because of the possible misinterpretations due to effects of radiation damage we adopted the procedure described in Campomenosi et al. (2020). Therefore, we included in the analysis only inclusions with full widths at half-maximum (FWHM) for the 1014 Raman band smaller than $\omega_{1014}^{FWHM} < 5.0$ cm^{-1}. The $\Delta\omega$ values of each mode of zircon and quartz inclusions and unstrained standards are listed in the repository database. Finally, sets of $\Delta\omega$ for each inclusion (modes ω_{128}, ω_{206}, and ω_{464} for quartz and modes ω_{342}, ω_{438}, ω_{969}, ω_{1014} for zircon, as they are generally unaffected by overlap with modes of the host garnet) have been used to determine strain using the software stRAinMAN (Angel et al., 2019) by employing the Grüneisen tensors for quartz (Murri et al., 2018) and zircon (Stangarone et al., 2019). The entrapment isomeke for quartz and zircon were obtained from their inclusion pressures with the online app EntraPT (Mazzucchelli et al., 2021), using the available equations of state for garnet endmembers (Angel et al., 2022), quartz (Angel et al., 2017) and zircon (Ehlers et al., 2022). The isomeke for pure garnet host endmembers were corrected for the mixed garnet composition using the approximation described in Angel et al. (2022) which assumes a linear dependency of the entrapment pressures of garnet endmembers.

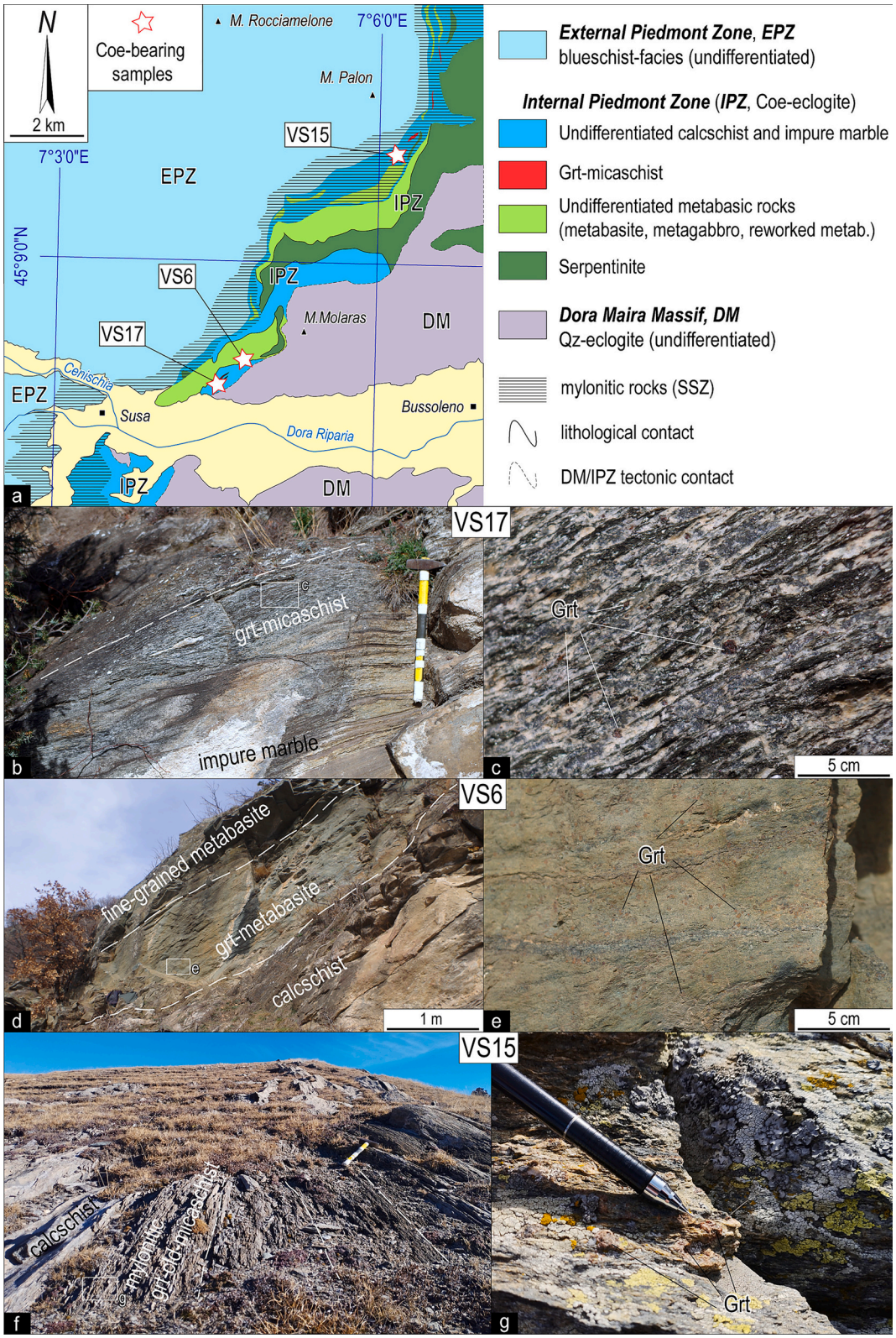

Fig. 2. a) Simplified geological map of the study area, modified after Ghignone et al. (2020b), Gasco et al. (2011). Stars indicate the sampling localities. Field occurrences of the different Coe-bearing rocks of Susa Valley. VS17 (45° 8′43"N; 7° 4'50"E) Grt-micaschist: b) outcrop setting, showing folding between Grt-micaschist and impure marble (hammer as scale); c) detail of the rock texture, with bigger garnet porphyroblast indicated. VS6 (45°8′52"N; 7°5′34″E) Grt-metabasite: d) outcrop setting showing a sharp stratigraphic contact (overturned) between Grt-metabasite and calcschist; e) detail of the rock texture, with bigger garnet porphyroblast indicated. VS15 (45°10′28"N; 7°7′9″E) Grt-Cld mylonitic micaschist: f) outcrop setting, showing a pervasive mylonitic foliation (hammer as scale); g) detail of the rock texture (pen as scale), with bigger garnet porphyroblast indicated (mineral abbreviations after Warr, 2021).

4. Field occurrence

The Internal Piedmont Zone in the mid-Susa Valley (locations in Fig. 2a) consists of a meta-ophiolitic basement with its metasedimentary cover. Here we focus on three specific lithotypes: garnet-micaschist (VS17), garnet-metabasite (VS6) and mylonitic garnet-chloritoid micaschist (VS15). Samples VS17 and VS6 are part of the thin portion of Internal Piedmont Zone pinned between the Dora-Maira at the bottom and the Susa-Shear Zone at the top (Fig. 2a). The structural setting of this sliver of meta-oceanic units is the result of at least four superposed ductile events, two of which (the most transpositive) formed by shearing-related isoclinal non-cylindrical folding, developed between the last subduction stages -including the one of the metamorphic peak- and the early exhumation steps (see details in Ghignone et al., 2020a, 2021a).

The Grt-micaschist VS17 outcrops as meter-thick layers of fine- to medium-grained (mm to few cm) quarzitic rocks alternating with carbonate-rich levels (Fig. 2b, c): it shows a well-developed mm-spaced foliation defined by alternating phyllosilicates- and quartz-rich levels. The Grt-metabasite VS6 crops out along a reverse fold limb geometrically above sample VS17 (Fig. 2a) within a 2–3 m thick sliver in contact with finer grained metabasites and calcschist (Fig. 2d). It is a medium-

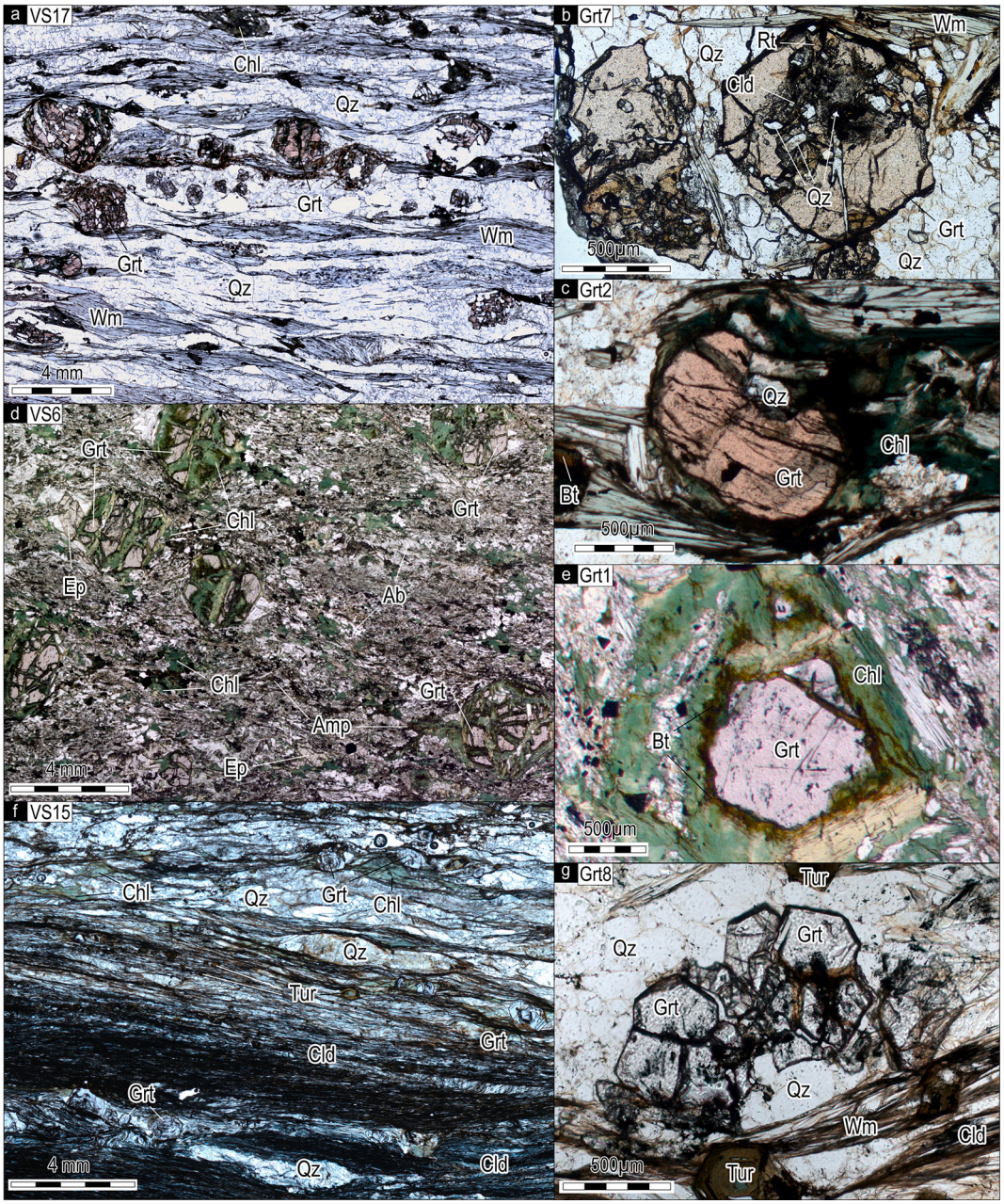

Fig. 3. Photomicrographs of the coe-bearing samples (Plane Polarized Light, PPL). VS17, Grt-micaschist: a) porphyroblastic texture of the sample, characterized by mm-sized garnet porphyroblast and quartz-mica-rich foliated matrix; b) strongly zoned garnet, whose textural zoning is defined by the large occurrence of inclusions in the core and less in the mantle; c) slightly zoned garnet, characterized by a low amount of inclusions. A weak decrease in its red colour from core to rim underline the chemical zoning. VS6, Grt-metabasite: d) porphyroblastic texture of the sample, characterized by mm-sized garnet relicts surrounded by a fine-grained matrix; e) relict garnet surrounded by chlorite and biotite. VS15, Grt-Cld mylonitic micaschist: f) porphyroblastic texture of the sample, characterized by mm-sized garnet porphyroblast and quartz-mica-chloritoid-rich mylonitic matrix; g) well-shaped and fractured garnet. (For interpretation of the references to colour in this figure legend, the reader is referred to the web version of this article.)

grained metabasic rock (Fig. 2d) with a cm-spaced foliation defined by oriented chlorite, green amphiboles and white mica wrapping cm-sized pre-kinematic garnet porphyroblasts (Fig. 2e).

The mylonitic Grt-Cld micaschist VS15 is from the Susa Shear Zone (Fig. 2f) and has a pervasive mylonitic foliation that partly transposes previous rock textures. Here, the lithotype crops out in lens-shape one meter- to few meters-thick bodies embedded within the shear zone (Ghignone et al., 2020a, 2020b). The intense shear zone deformation strongly overprints the original rock features and the best preserved pre-mylonitic relics occur within pre-kinematic garnet porphyroblasts (Fig. 2g).

5. Samples description

5.1. General petrography

5.1.1. Garnet-micaschist (VS17)

Sample VS17 is a garnet micaschist characterized by a pervasive foliation defined by mm-spaced alternating quartz- and phyllosilicate-rich domains (Fig. 3a). Quartz is dominant in the sample and the HP assemblage consist of garnet, phengite, chloritoid, and minor rutile. The rock was re-equilibrated in greenschist facies conditions and also contains chlorite, albite, muscovite and minor epidote, titanite and biotite (see Ghignone et al., 2021a, 2021b for a detailed sample description).

Garnet is wrapped by the foliation and shows core-to-rim chemical zoning. Two distinct garnet types are found based on their zoning patterns and on their occurrence in the rock: i) strongly zoned garnets exclusively concentrated in the quartz-rich levels (Figs. 3b, 4a), and ii) slightly zoned garnets concentrated instead in the mica-rich ones (Figs. 3c, 4b).

Strongly zoned garnets display three growth-shells (core, mantle and rim) characterized by a strong core-to-rim chemical variation (Fig. 4e): a wide spessartine (Sps)-rich core (almandine (Alm)$_{34–45}$, Sps$_{48–68}$, grossular (Grs)$_{4–6}$, pyrope (Prp)$_{2–3}$), a Alm-richer mantle (Alm$_{44–70}$, Sps$_{11–48}$, Grs$_{5–8}$, Prp$_{3–7}$) and a thin rim characterized by a strong reduction in Sps coupled with an increase in Alm and Grs (Alm$_{68–75}$, Sps$_{3–11}$, Grs$_{7–18}$, Prp$_{3–7}$).

Even the slightly zoned garnets exhibit three growth-shells (core, mantle and rim, Fig. 4f): homogeneous Alm-rich core (Alm$_{81–84}$, Sps$_{4–6}$, Grs$_{3–6}$, Prp$_{5–6}$), poorly developed mantle (Alm$_{80–82}$, Sps$_{3–4}$, Grs$_{6–10}$, Prp$_{5–6}$) and a tiny rim characterized by an increase in Grs at the expense of Alm content (Alm$_{72–80}$, Sps$_{4–5}$, Grs$_{10–20}$, Prp$_{4–6}$.

5.1.2. Garnet-metabasite (VS6)

The garnet-bearing metabasite VS6 is characterized by a weak foliation defined by isooriented phyllosilicates and tabular-shaped minerals. The rock has a typical greenschist facies assemblage of chlorite, epidote, green amphibole, poikiloblastic albite and muscovite (Fig. 3d).

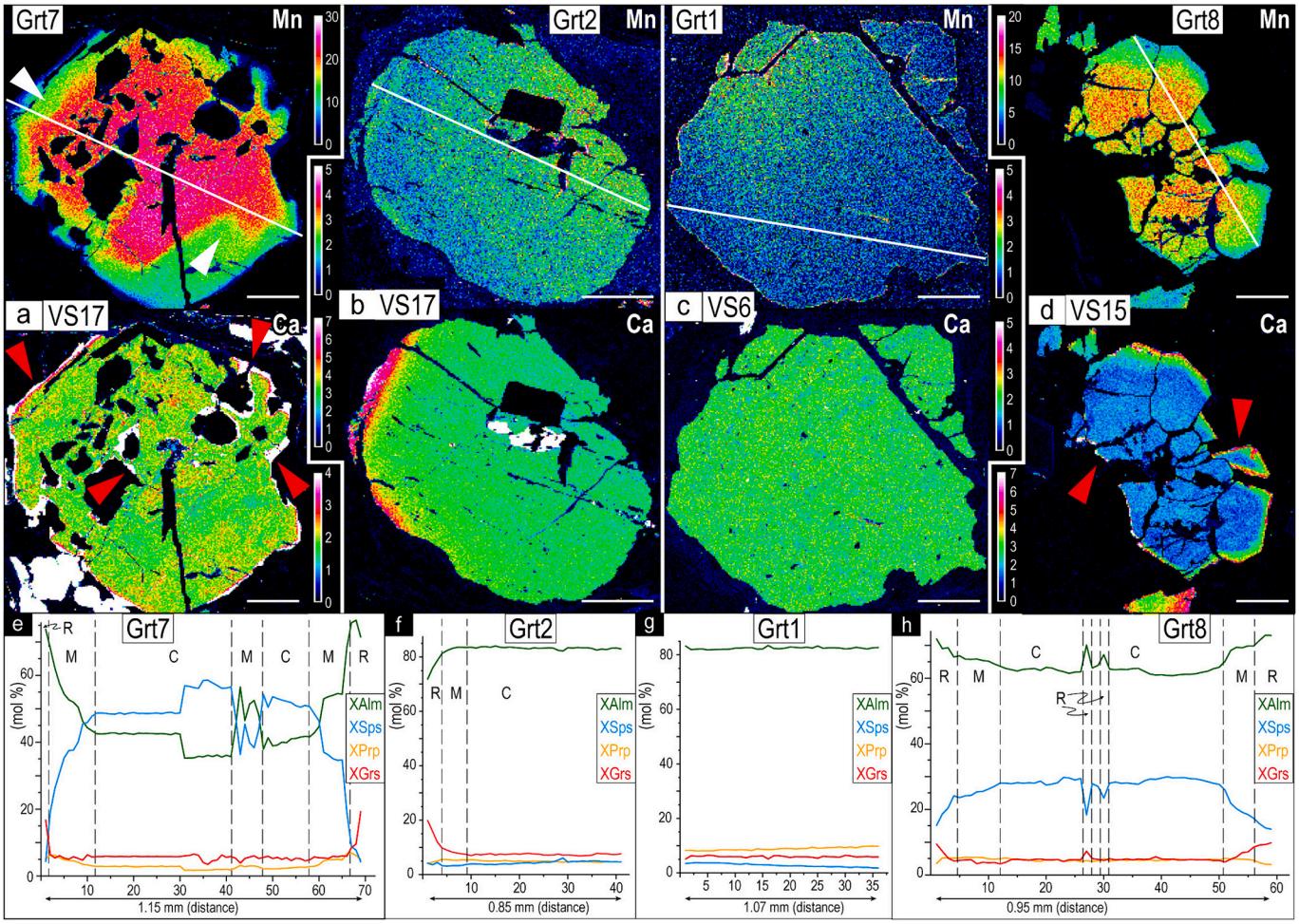

Fig. 4. Chemical characterization of the garnets: X-Ray maps (Mn and Ca) of selected garnets in a) VS17, Grt7, b) VS17, Grt2, c) VS6, Grt1, d) VS15, Grt8. White lines show the orientation of the profile whereas the white scale bar is 200 μm in each picture. White arrows indicate the gulf-shape of the core zoning (VS17-Grt7). Red arrows indicate the Ca-rich rims growth around garnet fragments after their cracking (VS17-Grt7 and VS15-Grt8). Compositional profiles of the same selected garnets: e) VS17, Grt7, f) VS17, Grt2, g) VS6, Grt1, h) VS15, Grt8. C, M, R are: core, mantle and rim. (For interpretation of the references to colour in this figure legend, the reader is referred to the web version of this article.)

Rare relicts of a previous higher-pressure metamorphic assemblage include partly re-equilibrated garnet porphyroblasts (Fig. 3e), phengite and rutile.

Centimetric garnet porphyroblasts (Figs. 3e, 4c) are enveloped in a greenschist facies foliation. They are strongly fractured and re-equilibrated in chlorite and biotite. Preserved garnet fragments are relatively fresh and with a near constant composition ($Alm_{82–84}$, $Sps_{2–4}$, $Grs_{5–7}$, $Prp_{8–10}$; Fig. 4g).

5.1.3. Garnet-chloritoid mylonitic micaschist (VS15)

Sample VS15 is a garnet-chloritoid micaschist characterized by a pervasive mylonitic foliation, which wraps mm-sized, fractured garnet porphyroblasts (Fig. 3f). The rock displays a well-preserved HP eclogite-facies assemblage characterized by garnet, phengite, chloritoid and rutile, and a LP greenschist facies assemblage with chlorite and muscovite (see Ghignone et al., 2021a, 2021b for a detailed sample description).

Garnet shows a slight core-to-rim compositional zoning (Figs. 3g, 4d) consisting of an Alm and Sps-rich core ($Alm_{61–64}$, $Sps_{27–30}$, $Grs_{4–6}$, $Prp_{4–5}$), a mantle slightly poorer in Sps ($Alm_{64–69}$, $Sps_{18–28}$, $Grs_{4–7}$, $Prp_{4–5}$), and a Grs richer thin rim ($Alm_{69–75}$, $Sps_{14–18}$, $Grs_{7–10}$, $Prp_{3–4}$, Fig. 4h).

5.2. Coesite inclusions in garnet

Coesite occurs exclusively within garnet core in all samples, either as isolated pristine inclusions (Fig. 5a, b, c, d) or within polycrystalline quartz aggregates surrounded by radial cracks (Fig. 5e). Pristine coesite inclusions (10–40 μm) are completely embedded in garnet, without any evidence of re-equilibration, and show sub-rounded (Fig. 5c, d) to polyhedral morphology (Fig. 5a, b). The measured Raman spectra (Fig. 5f and Tables S2 and S3) show the typical vibrational modes of the phase (Boyer et al., 1985), but slightly shifted to the right due to the inclusion being pressurized (Fig. 5g). The main Raman band is located at 523 cm^{-1} (instead of 521 cm^{-1}, Boyer et al., 1985), and the secondary ones at 427, 271 and 180 cm^{-1}.

Pseudomorphs after coesite consist of quartz with polycrystalline texture surrounded by radial cracks in garnet host starting from the inclusion corners and edges (Fig. 5e, h, e.g., Chopin, 1984). These cracks display the typical shape linked to the sharp volume increase of the transformation of coesite into quartz (Bose and Ganguly, 1995). Partly re-equilibrated inclusions preserve a core of coesite surrounded by polycrystalline quartz (Fig. 5e, h). In general, the inclusions with quartz pseudomorphs after coesite appear to be larger than pristine coesite inclusions (Fig. 5i, inclusion in Fig. 5h).

5.3. Inclusions distribution in garnet

In the previous section we reported the presence of coesite in garnet cores. Here we describe the distribution and mineralogy of the various other type of inclusions present in the different garnet shells to collect fundamental information on the metamorphic conditions of garnet growth (Table 1 and Fig. 6). Inclusions were identified via μ-Raman spectroscopy and microprobe. Both garnet types from sample VS17 include SiO_2 polymorphs, chloritoid, phengite, amorphous carbon, rutile, florencite (i.e., REE-rich Al-phosphate, Ghignone et al., 2023b) and zircon (Fig. 6a, b). Only in the core, garnets include coesite, paragonite+epidote and albite+muscovite+paragonite±biotite aggregates, pseudomorphic after former lawsonite and jadeite, respectively (see Groppo et al., 2019).

In sample VS6 garnets include ubiquitously pristine coesite, rutile, zircon, apatite, florencite, rare tourmaline, and paragonite+epidote pseudomorphs after lawsonite (Fig. 6c).

In VS15 sample, garnet contains SiO_2 polymorphs, chloritoid, phengite, amorphous carbon, rutile, zircon, florencite and minor xenotime. As for VS17, coesite, paragonite+epidote pseudomorphs after lawsonite and albite+muscovite+paragonite±biotite pseudomorphs after jadeite occur only in garnet cores (Fig. 6d). Garnet mantles and rims of all samples are instead dominated by quartz occurring either as single crystals or as polycrystalline aggregates (Fig. 6). In VS17 and VS15, quartz occurs also in big patches (> 80 μm) and as filling of cracks (Fig. 6a, b, d).

6. PT estimates of garnet growth

6.1. Elastic geobarometry (EGB)

The elastic barometry calibrations are based on the principle that the inclusion strain can be measured with Raman spectroscopy and then converted into inclusion pressure with the available elastic tensors (Wang et al., 2015 for quartz, Özkan et al., 1974 for Zircon). Knowledge of the inclusion pressure and the thermodynamic properties of host and inclusion (i.e., their equation of state, EoS) allows to calculate the isomeke, a line in P-T space along which the change in volume of the pair remain constant (Angel et al., 2014). We applied EGB in the study area to test its reliability and compare the results with well-constrained P-T estimates obtained with thermodynamic and conventional thermobarometry.

The results of Raman spectroscopy on quartz (sample VS15) and zircon (samples VS6, 15, 17) inclusions in garnet are shown in Fig. 7 and in the repository datafile (Supplementary Table S2). The inclusion strain is given with its 2σ confidence ellipse in Fig. 7. The strain of quartz inclusions in near-hydrostatic, with very elongated 2σ confidence ellipse subparallel to the lines of equal P_{inc} (in black). The strain of zircon inclusions ranges from near hydrostatic (sample VS6) to strongly anisotropic (samples VS15 and VS17). Nevertheless, all zircon inclusions plot along the same line of equal Pinc, within their 2σ uncertainties.

In sample VS15, the inclusion pressure of quartz in garnet mantles and rims appears consistent within uncertainty. This allows to assume that all quartz inclusions within each growth zone were entrapped at the same P-T conditions (Fig. 7a, c). The inclusion pressures were therefore averaged (least-square weighted average) to obtain a representative quartz inclusion pressure for each growth zone (thick lines in Fig. 8a). The same is true for zircon inclusions, which show similar inclusion pressures within the same sample considering their uncertainties (Fig. 7b, d). We therefore obtained a representative zircon inclusion pressure for each of the three analyzed samples (thick lines in Fig. 8b).

The average inclusion pressure (Pinc) of quartz inclusions from sample VS15 suggests the occurrence of two stages of garnet mantle growth: inner mantle (Pinc = 1.04 ± 0.07; 2σ error) and outer mantle (Pinc = 0.85 ± 0.05). Garnet inner mantles formed at around 2.3 ± 0.2 GPa (T = 520 °C) and outer mantles formed at 1.9 ± 0.2 GPa (T = 520 °C). These estimates are consistent with results from Ghignone et al. (2021a). The average inclusion pressures of zircons from sample VS6 and VS17 give consistent temperature estimates of about 550 ± 25 °C at 1 GPa and 750 ± 25 °C at 3 GPa. Zircons from sample VS15 suggest slightly higher equilibration temperatures to 600 ± 25 °C at 1 GPa and 800 ± 25 °C at 3 GPa.

6.2. Zr-in-rutile geothermometry

The Zr content in rutile included in garnet provides valuable information about the temperatures of entrapment. Rutile inclusions in garnet are widespread in all three samples. However, only in sample VS15 the inclusions have an area exposed to the sample surface wide enough to allow for unmixed analyses. In this sample rutile are included in every garnet shell, they are well-preserved and unaffected by the typical titanite re-equilibration observed in rutile crystals from the rock matrix. Zirconium content was measured with the microprobe and most of the crystals analyzed had a similar mean Zr content (~21 ppm). Temperatures were estimated using the pressure dependent Zr-in-rutile calibration proposed by Kohn (2020). The results are consistent within

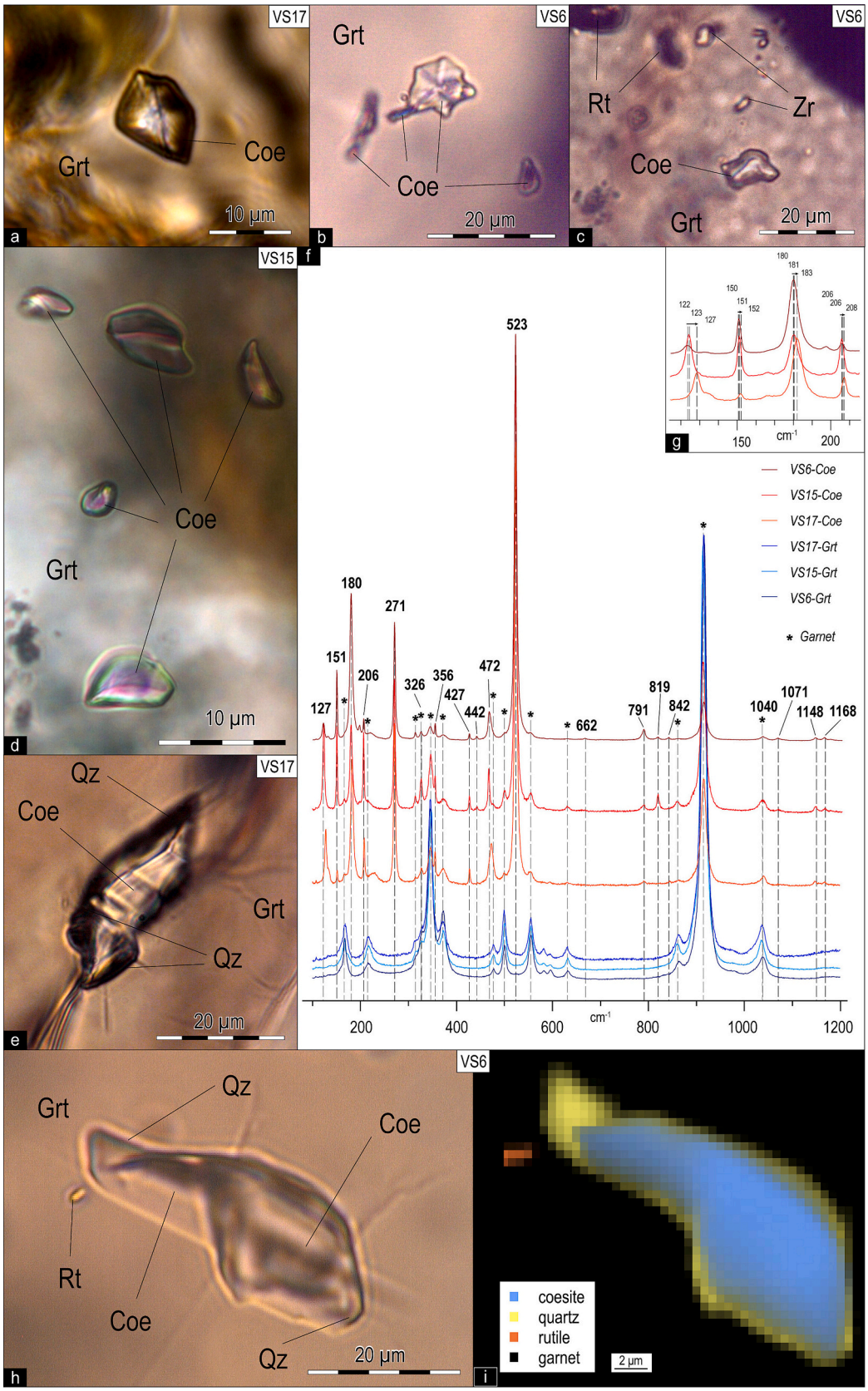

(caption on next page)

Fig. 5. Close-up images in PPL of coesite (and other phases) inclusions in garnet from the studied samples. a) and b) pristine coesite inclusions showing polyhedral morphology. c) and d) pristine coesite inclusions showing sub-rounded shape. e) Coesite inclusion partly re-equilibrated in quartz along a fracture. f) Raman spectra of coesite and garnet from the three analyzed samples. Peaks marked with the value (cm^{-1}) are assigned to coesite, while peaks marked with asterisk are referred to garnet host. Garnet marked peaks values: 168, 216, 315, 328, 348, 371, 477, 500, 555, 630, 861, 914 and 1038 cm^{-1}. Please note that 326 and 1040 cm^{-1} peaks are shared between garnet and coesite. g) Detail of the superposed coesite Raman spectra, showing peaks with a significant Raman shift. h) Coesite inclusion partly re-equilibrated in quartz. Please note the incipient radial cracks around the inclusion. j) Raman map of the inclusion in i), showing coesite (pale blu) surrounded by a thin rim of quartz (yellow). Note the thin radial cracks protruding from the inclusion into the host garnet Garnet (black) and rutile (orange) are also shown. (For interpretation of the references to colour in this figure legend, the reader is referred to the web version of this article.)

Table 1
Mineral assemblage stable with the different garnet shell of each garnet type in the investigated samples (VS17, VS6, VS15).

sample	VS17						VS6	VS15		
lithotype	Grt-micaschist						Grt-metabasite	Mylonitic Grt-Cld micaschist		
Grt main features	Strongly zoned			Slightly zoned			Unzoned	Zoned		
	core	mantle	rim	core	mantle	rim		core	mantle	rim
coesite	■			■			■	■		
quartz		■	■		■	■			■	■
chloritoid	■	■	■	■	■	■		■	■	■
rutile	■	■	■	■	■	■	■	■	■	■
lawsonite	■			■			■	■		
jadeite	■			■				■		
phengite	■	■	■	■	■	■		■	■	■
am. carbon	■	■	■	■	■	■		■	■	■
zircon	■	■	■	■	■	■	■	■	■	■
florencite	■	■	■	■	■	■	■	■	■	■
apatite							■			
tourmaline							■			
xenotime							■			

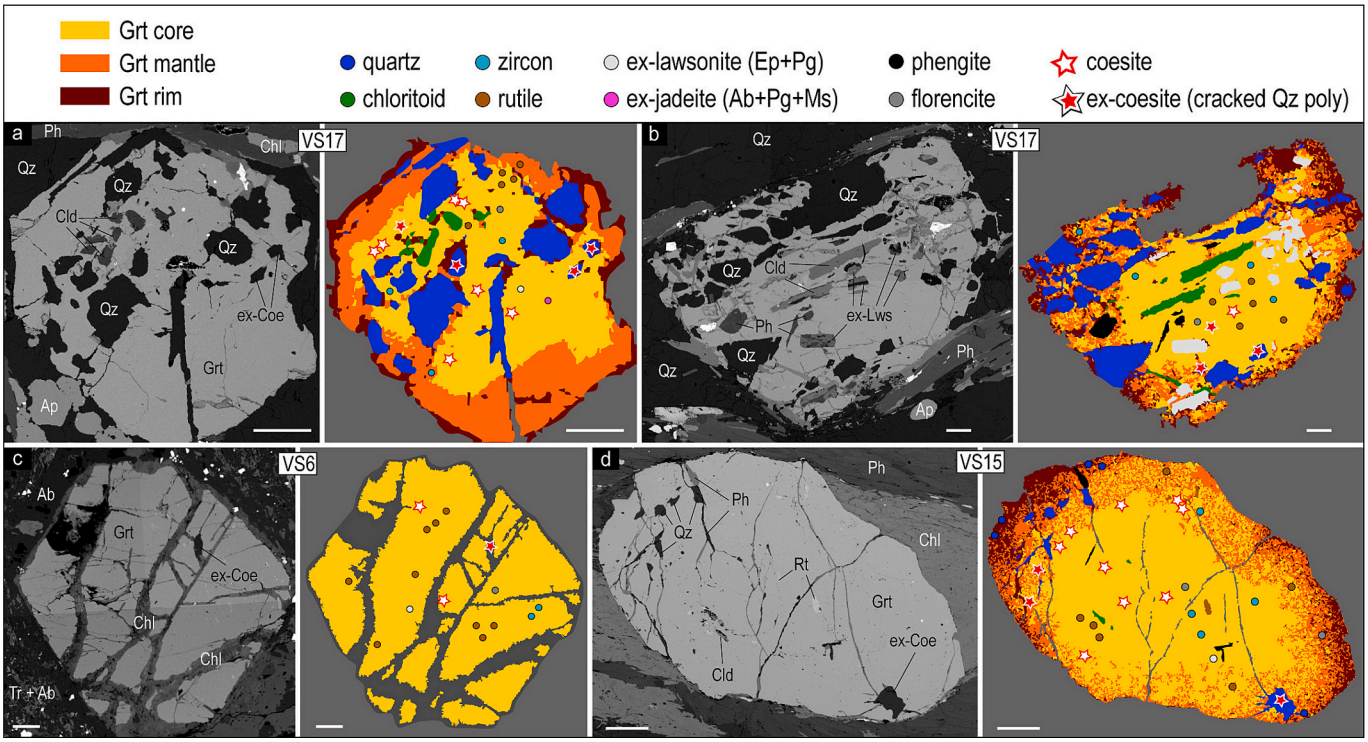

Fig. 6. Simplified drawing of garnets based on real zoning defined via X-Ray maps of each sample and their BSE image a), b) VS17 (both garnet compositional generations), c) VS6 and d) VS15, showing inclusion distribution within each different compositional shell. Larger inclusions cropping out from the section surface are coloured (see legend), while coloured dots represent inclusion detected via μ-Raman below the section surface. Bar scale in each picture is 200 μm.

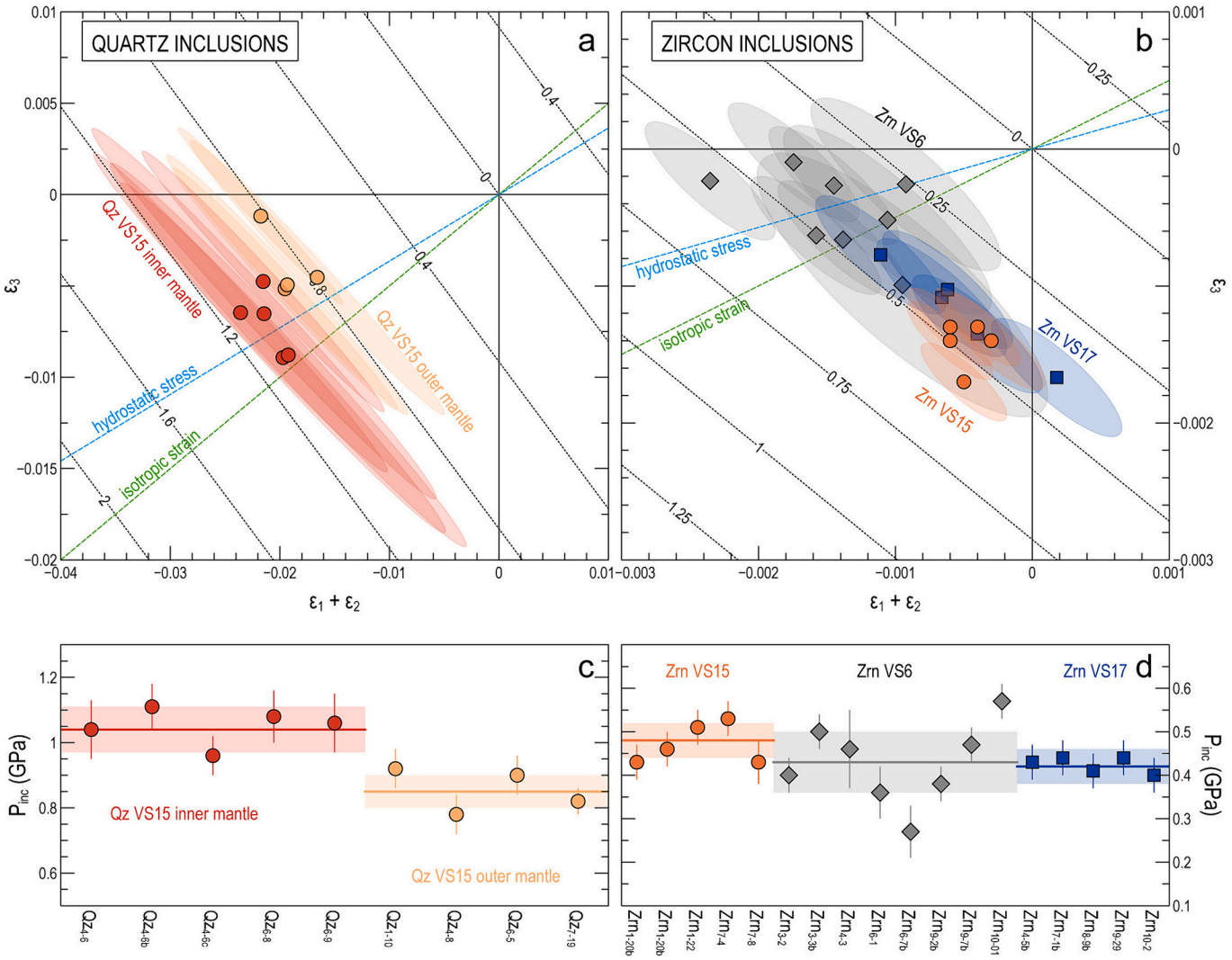

Fig. 7. (ε1 + ε2) vs ε3 plots showing residual strain estimated for each sample. Strains and inclusion pressures of quartz (a and c) and zircon (b and d) inclusions in garnet from samples VS15, VS6 and VS17. The symbol colour indicates the occurrence of such inclusions within VS15 garnet inner (in red; only quartz) and outer mantles (in orange; quartz and zircon), and zircons in garnet from sample VS6 (in grey) and VS17 (in blue). The strain diagrams (a and b) also include the lines of equal Pinc, of isotropic strain and of hydrostatic stress (i.e. the Reuss and Voigt boundaries) for quartz (a) and zircon (b). The shaded ellipses in (a) and (b) are 1-sigma uncertainties on strain and indicate that the uncertainty on inclusion pressure calculated from the strain is relatively small compared to the strong dependency between the two axial strains. The horizontal lines and shaded areas in (c) and (d) are the inverse variance weighted average and uncertainty of the inclusion pressure and are representative of the garnet growth zones. (For interpretation of the references to colour in this figure legend, the reader is referred to the web version of this article.)

uncertainties, providing an average temperature ranging from 420 ± 10 °C at 1.0 GPa - obtained using the equation for the α-quartz field- to 502 ± 10 °C at 2.8 GPa - obtained instead using the equation for the coesite field (Fig. 8). Kohn (2020) calibration was chosen because it is pressure dependent and based on more solid data (experimental and natural samples) with respect to older calibrations. In addition, Kohn (2020) presents a wide discussion on the reliability of the different calibrations.

7. Discussion

7.1. Garnet growth and evolution

In sample VS17, two garnet types were recognized based on colour, grain size and chemical composition (see Figs. 3 and 4). Both types are located in the same microstructural positions, i.e., both wrapped by the same foliation, and contain the same sets of inclusions distributed in same shells with coesite placed in the garnet core. Therefore, they can be interpreted as coeval and their chemical differences can be ascribed to primary local bulk variations of the protolith (see e.g., Lanari and Engi, 2017). The compositional homogeneity of slightly zoned garnet may be the result of intra-crystalline diffusion which acted during subsequent re-equilibration of the rock. However, the low temperatures recorded by the rock and the existence of a generation of garnets exhibiting strong compositional zoning suggest that intra-crystalline diffusion is negligible during the growth and subsequent re-equilibration of the garnet (see e.g., Carlson, 2006).

Both garnet types in VS17 show (i) an episode of resorption/reprecipitation followed by (ii) an episode of brittle fracturing (white and red arrows, respectively, in Fig. 4a). Resorption occurred after the garnet core growth, testified by its gulf-shaped and lobed morphologies of the chemical zoning (see e.g., Rubatto et al., 2020; Fig. 4a), and sealed by the subsequent growth of garnet mantle. The brittle fracturing occurred after the garnet mantle growth, as suggested by zoned garnet fragments. After the fracturing, garnet rim partly seals the cracks that separate the garnet fragments (Fig. 4a).

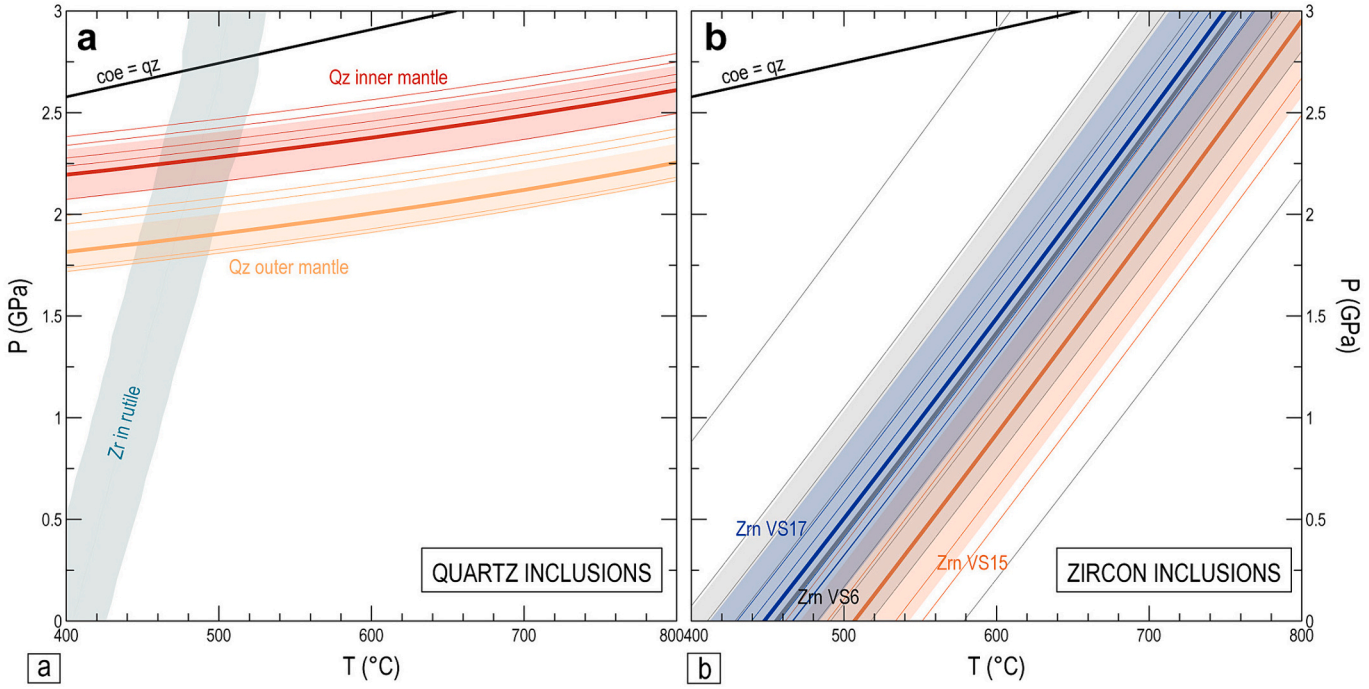

Fig. 8. Calculated isomeke for a) Qz inclusions in sample VS15, b) Zr inclusions in each sample (VS17, VS6, and VS15). Isomeke of (a) quartz in garnet from sample VS15 (inner mantle in red and outer mantle in orange) and (b) zircon in garnet from sample VS15 (outer mantle in orange), VS6 (in black), and VS17 (in blue). The thicker lines and their shaded areas are the isomeke calculated using the average inclusion pressure for the garnet zones with their 2-sigma uncertainties. The thinner lines are the isomeke calculated for each single inclusion. In (a) quartz-in-garnet isomeke are crossed with the temperature estimates from Zr-in-rutile thermometry (blue shaded area). The quartz-coesite transition line (coe = qz, in black) is from (Bose and Ganguly, 1995). (For interpretation of the references to colour in this figure legend, the reader is referred to the web version of this article.)

The absence of a significant chemical zoning in garnets of the sample VS6 might be the result of the substitution of the original zoned garnet rim by chlorite and biotite (Fig. 3e).

In analogy with garnets of VS17 sample, the slight garnet zoning observed in sample VS15 may be mainly due to a continuous growth process with just a negligible contribution of intra-crystalline diffusion. In addition, brittle fracturing after the growth of garnet mantle occurred also in garnets of VS15 and the different garnet fragments are sealed by garnet rim growth (white arrows in Fig. 4d). According to EGB results for quartz in garnet the brittle event took place at $P < 1.8$ GPa, during exhumation.

7.2. *Metamorphic evolution of coe-bearing Internal Piedmont Zone in the Susa Valley*

Results obtained combining detailed inclusions analyses in zoned garnets with the EGB and Zr-in-rutile geothermometry provide new constraints for a better determination of the P-T evolution of the coesite-bearing meta-ophiolites in the Susa Valley. Each metamorphic stage was compared with the existing thermodynamic results proposed by Ghignone et al. (2021a).

The preservation of coesite in garnet-cores of samples VS17 and VS15 confirms the peak-P for the Internal Piedmont Zone in the Susa Valley above the Coe-Qz transition (Fig. 9). In VS6 garnets are homogeneous in composition and coesite is widespread; therefore, the whole garnet can be ascribed to a unique metamorphic event, i.e., peak-P in UHP conditions. The presence of coesite suggests that the peak-P for the whole set of samples is $P > 2.8$ GPa. At this pressure the Zr-in-rutile geothermometer in garnet cores yield a T ~ 500 °C (Point 1 in Fig. 9), consistent with the results obtained with thermodynamic modelling by Ghignone et al. (2021a, M1a stage). The Zr-content in rutile crystals is constant within uncertainty (21 ± ppm). This suggests that rutile grew in a single metamorphic stage, before or during garnet growth. Therefore, it likely provides an indication of the minimum temperature for garnet core growth rather than the true peak temperature.

After the peak-P, the Internal Piedmont Zone followed a slightly prograde to nearly isothermal decompression event, still at HP conditions (M1b of Ghignone et al., 2021a), whose pressure was constrained using Qz in garnet isomeke from sample VS15 (Fig. 9). We identified two points (P = 2.25–2.3 GPa and 1.85–1.9 GPa) in which the calculated isomeke intersect the thermodynamically calculated P-T path (Point 2a and 2b in Fig. 9). These two points mark two stages of garnet mantles growth (sample VS15) recorded by Qz inclusions entrapment at different P during the exhumation path.

The post eclogite facies re-equilibration was observed in all samples and corresponds to the formation of the greenschist facies mineral assemblage (LP-LT) as proposed by Ghignone et al. (2021a) (point 3? in Fig. 9). However, no precise quantitative P-T conditions for this stage are available.

An additional stage was recognized using zircon in garnet EGB. Zircon inclusions generally reset during the retrograde path because of tensile stresses developing in the host garnet around the inclusion at high temperatures, and record the maximum temperature reached by the system at the lowest pressure, i.e., the point in P-T space where the system switches from decompression to cooling (Campomenosi et al., 2021, 2023; Mingardi et al., 2023). The resulting isomeke crosses the P-T path at low pressure (~ 0.4–0.5 GPa) and relatively higher temperature (530–540 °C; point 4 Fig. 9). In particular, the average inclusion pressures of zircons from sample VS6 and VS17 give consistent temperature estimates around 520–530 °C (~ 0.4–0.5 GPa). Zircons from sample VS15 suggest slightly higher equilibration temperatures to 530–550 °C (~ 0.4–0.5 GPa). This variation in T may be due to the slightly different position of the samples (Fig. 2a). In fact, VS6 and VS17 occur adjacent to each other, whereas VS15 occurs ~10 km apart and was teared from its original position by the Susa Shear Zone, which might have played a role in the late heating.

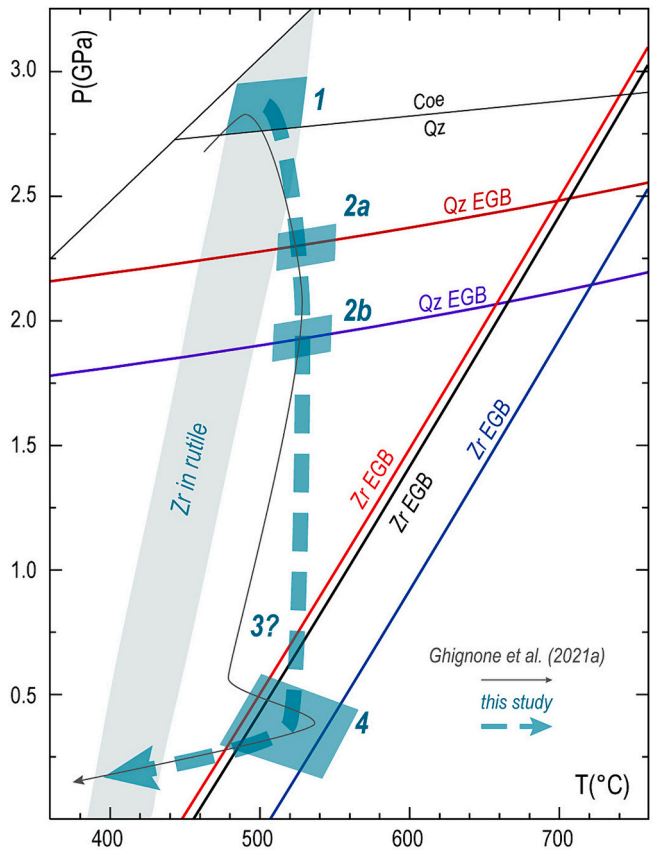

Fig. 9. P-T path obtained for the Internal Piedmont Zone in the Susa Valley (dashed green path) compared with the P-T path (tiny grey path) calculated by Ghignone et al. (2021a). See text for details. (For interpretation of the references to colour in this figure legend, the reader is referred to the web version of this article.)

In summary, the P-T path (Fig. 9) can be described as follow. The samples after a peak at UHP conditions (point 1 Fig. 9) was slightly heated during decompression while still at eclogite facies conditions (point 2 Fig. 9). Subsequently, the rock follows a near-isothermal decompression towards lower pressure conditions at the boundary between greenschist and amphibolite-facies (point 4 Fig. 9). Precise P and T conditions of the greenschist facies assemblage are difficult to quantitatively estimate. However, the formation of this assemblage takes place prior to stage 4 reported in Fig. 9. The discovery of coesite and the application of EGB and conventional thermometry support and pinpoint the different stages of the samples evolution already modelled by Ghignone et al. (2021a).

7.3. Coesite occurrence in the Western Alps

Coesite findings are rare because often the samples are re-equilibrated and prediction of its presence are only based on thermodynamic modelling (e.g., Angiboust et al., 2012; Ghignone et al., 2021a). Coesite forms via a metamorphic reaction that mobilize SiO_2 at UHP conditions and can be trapped and preserved when garnet is growing simultaneously. Once trapped the preservation of coesite totally depends on how well the system remains closed. If coesite is entirely surrounded by garnet, its back-transformation to quartz is inhibited by garnet, that behaves as P-shield. The pressure that a coesite inclusion, totally sealed in garnet, experiences is lower than the external one, so the re-equilibration may not take place (Gilio et al., 2022). In addition, to preserve coesite the garnet should not endure re-equilibration or intense fracturing. Another key point is the grain size of the coesite inclusions. Several authors (e.g., Chopin, 1984; Liou et al., 2012; Reinecke, 1991; Zhang et al., 2002) described worldwide coesite crystals as >50–60 μm, always partly re-equilibrated. Recently, also small (< 50 μm) and rather fresh inclusions of coesite without any evidence of re-equilibration were described (Ghignone et al., 2023a; Manzotti et al., 2022; Schönig et al., 2022; Taguchi et al., 2021; Xiong et al., 2021) suggesting that the crystal size might play a role. In fact, it is known that the rheological behaviour of the garnet is influenced by the inclusions size (e.g., Mazzucchelli et al., 2018 and references therein).

The coesite inclusions in the Internal Piedmont Zone have similar features and were found as both small and pristine crystals, as well as large and partially re-equilibrated grains. However, the host rock differs: in the Susa Valley coesite occurs in micaschists and metabasites (this work), at Lago di Cignana in Mn-bearing quarzites and metabasites (Reinecke, 1991; Taguchi et al., 2021)and in Lago Superiore in the Grt-micaschists (Ghignone et al., 2023a).

All the different coesite discoveries (the one of this manuscript included) in the Western Alps makes the locality at UHP conditions more widespread than previously thought. The presence of coesite also in Susa Valley makes this statement particularly true for the garnet-bearing metasediments of the Internal Piedmont Zone.

7.4. Tectonic implications

The UHP Susa Valley unit crops out in the same structural position of the Lago di Cignana and Lago Superiore UHP units (Ghignone et al., 2023a; Reinecke, 1991). They all show similarities - within uncertainties - in peak-P conditions, laying on the same metamorphic gradient (5–6 °C/km, Fig. 10a) and depth range. The resulting gradient, on which the three UHP meta-ophioites units of the Western Alps lay, is colder with respect to that recorded for other meta-ophiolites units (e.g., Zermatt-Saas Unit, Fig. 10a) whose peak-PT conditions are not in the UHP field (Brown, 2023). Although the peak-P conditions calculated for Lago di Cignana Unit (Groppo et al., 2009) are slightly higher with respect to the one of the other two units, this discrepancy can be explained by geometrical variation and/or orientation of the alpine Tethyan slab (Fig. 10b; Agard and Handy, 2021). Moreover, the portion of the Internal Piedmont Zone in the Susa Valley represents the northern prosecution of the southern UHP Lago Superiore Unit. The Lago di Cignana Unit might be the continuation of the same tectonic unit to the north.

With this new discovery and considering the similarities of the three units we infer that they likely represent slices of a former UHP level within the Internal Piedmont Zone (Fig. 10b). This assumption is supported by the geochronological data, in fact the peak UHP metamorphism was dated to ~50–45 Ma in all three units (Lago di Cignana: Gouzu et al., 2016; and Rubatto et al., 1998; Lago Superiore: Angiboust and Glodny, 2020; and Rubatto and Hermann, 2003; Susa Valley: Ghignone et al., 2021b). The dismembering of this UHP level may have occurred during exhumation, most likely at blueschist-greenschist facies conditions. This hypothesis is based on the field relationships between the different tectonic slices of the Internal Piedmont Zone (see e.g., Angiboust and Glodny, 2020) and on the fact that this Zone is partially discontinuous at the orogen scale (see Fig. 1). Furthermore, the remarkable similarities in the T/P gradient of these units (Fig. 10a) along 150 km length slab interface tends to exclude the localized non-lithostatic pressure conditions (e.g., overpressure; see e.g., Mancktelow, 1993; Tajčmanová et al., 2021) as an efficient process to explain this peak P-T values.

The broad occurrence of coesite within the Internal Piedmont Zone increases the extension of the UHP units (Figs. 1, 10b), making the model of a localized non-lithostatic pressure difficult to apply to the oceanic units of the Western Alps.

In addition, conventional buoyancy driven exhumation models (i.e., thermodynamic studies) in cold subduction zones have indicated a threshold of ~80 km as the maximum depth of recovery for the exhumation of the oceanic crust (see e.g., Chapman et al., 2019). The

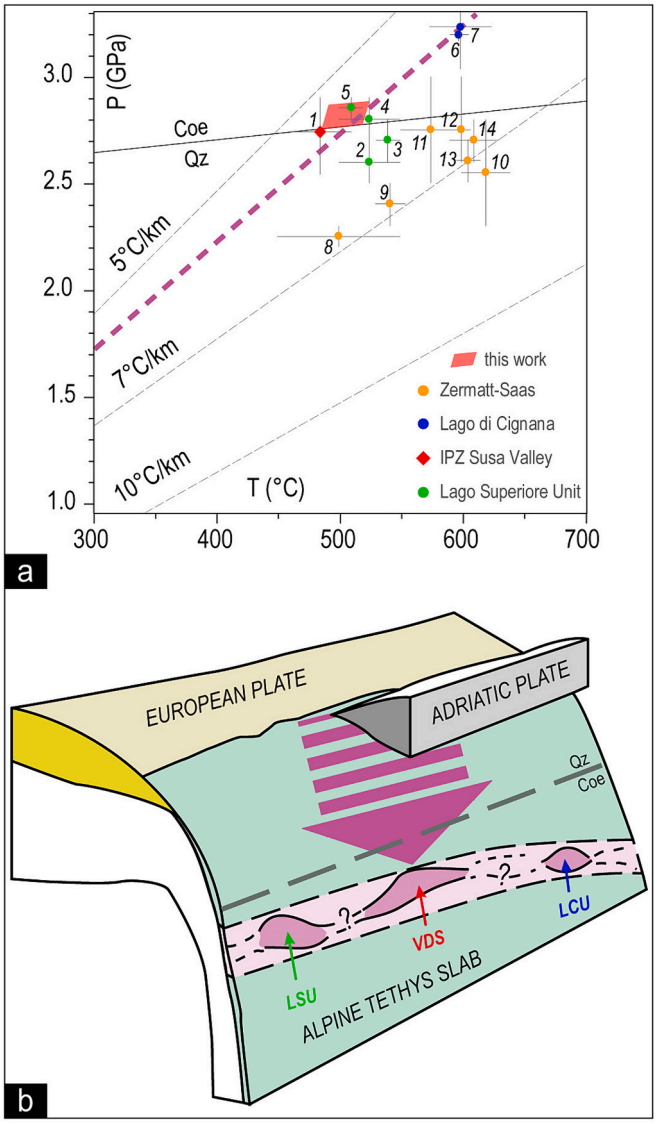

Fig. 10. a) Peak-PT of the three UHP meta-ophiolites of the Western Alps compared with the Qz-eclogite facies meta-ophiolites of the Zermatt-Saas Unit. Numbers refer to the following works: 1 Ghignone et al. (2021a); 2 Angiboust et al. (2012); 3 Locatelli et al. (2018); 4 Gilio et al. (2020); 5 Ghignone et al. (2023a); 6 Groppo et al. (2009); 7 Frezzotti et al. (2014); 8 Weber and Bucher (2015); 9 Angiboust et al. (2009); 10 Zanoni et al. (2016); 11 Bucher et al. (2005); 12 Groppo et al. (2009); 13 Bucher and Grapes (2009); 14 Skora et al. (2015). Colours referred to each locality: green for Lago Superiore Unit; red for Susa Valley; blue for Lago di Cignana Unit; orange for Zermatt-Saas Unit). b) Schematic sketch (not to scale) of the Alpine subduction zone, showing the relative position of the different UHP localities within the oceanic slab. LSU = Lago Superiore Unit; VDS = Susa Valley Unit; LCU = Lago di Cignana Unit. (For interpretation of the references to colour in this figure legend, the reader is referred to the web version of this article.)

proposed model of exhumation, involving the off-scraping of coherent and continuous oceanic crust along a subduction interface from depths of ~100 km to the surface, challenges the conventional buoyancy-driven exhumation models. Accordingly, buoyancy-driven forces might not represent the main mechanism for the exhumation of the Internal Piedmont Zone.

8. Conclusions

Combining different techniques (Elastic Geothermobarometry, inclusions in garnet distribution, zircon in rutile geothermometry) and comparing the results with thermodynamic modelling available for the area (Ghignone et al., 2021a), we provide a better constrain of the metamorphic evolution of the coesite-bearing rocks of the Susa Valley unit.

Our new coesite finding in Susa Valley represent an additional missing piece of solid evidence that -together with the recent finding in Lago Superiore (Ghignone et al., 2023a) and the one in the 90s in Lago di Cignana- supports the interpretation that the subduction of the oceanic crust reached UHP conditions along the same gradient, roughly synchronously. We argue that the Internal Piedmont Zone was subducted at a depth of almost 100 km and experienced a roughly uniform metamorphic evolution along the entire Western Alps.

Further structural mapping of the meta-ophiolites of the Internal Piedmont Zone will fill the gap of an accurate and detailed distribution of the UHP unit.

The broad occurrence of coesite within the Internal Piedmont Zone challenges conventional buoyancy-driven exhumation models.

The UHP oceanic units worldwide are definitely two to date, the Western Tianshan and the UHP-Internal Piedmont Zone, that is represented by slices of a former unique UHP slice, now dismembered.

Coesite in the Western Alps is more widespread than previously thought. We believe that several other coesite-bearing UHP localities will be discovered in the years to come.

Fundings

The research has been funded as follow: SG, MB and FB were supported by research grants from University of Torino, Ricerca Locale 2022 (Cdd. 21/07/2022); AB was supported by the German Federal Ministry for Education and Research and the Deutsche Forschungsgemeinschaft (projects FE 1527/2-3 and FE 1527/4-1 to Silvio Ferrero) and partly co-funded by the National Science Center (Poland) and the European Union Framework Program for Research and Innovation Horizion 2020 under the Marie Skłodowska-Curie grant agreement No. 945339 (project no. 2021/43/P/ST10/03202); MG was supported by the Alexander von Humboldt Foundation (Bonn, Germany) and by the projects High-stress Earthquakes by Faulting in Deep Dry Rocks (THALES, PRIN-MIUR N. 2020WPMFE9 to G. Pennacchioni) and Development of Digital TWIns for multiphysics simulation of eXtreme events in civil engineering (DTWI, PRIN-MIUR N. 2022AL5MSN to M. Cremonesi).

Author contributions

Conceptualization: SG, MG, ES, AB, MB; Investigation: SG, MG, ES; Data curation: SG, MG, FB, AB, ES; Methodology: SG, MG, ES, AB, FB, MB; Supervision: MB; Validation: SG, MG, ES, AB, MB; Writing – original draft: SG, ES; Writing – review & editing: SG, MG, ES, AB, FB, MB. All authors read and approved the final manuscript.

Declaration of competing interest

The authors declare no competing or conflicting interests.

Acknowledgments

We thank the editor N. Malaspina, C.E. Ganade and two anonymous reviewers for their critical and constructive reviews. We are warmly thankful to F. A. Livio, M. Gattiglio, A. Borghi and M. Alvaro for their contribution in discussing the geological implications of our discovery, to M. Scambelluri for comments on an early version of this manuscript and to C. Günter and C. Fischer for help with analyses and sample preparation.

Appendix A. Supplementary data

Supplementary data to this article can be found online at https://doi.org/10.1016/j.lithos.2024.107575.

References

Agard, P., 2021. Subduction of oceanic lithosphere in the Alps: selective and archetypal from (slow-spreading) oceans. Earth-Sci. Rev. 214, 103517 https://doi.org/10.1016/j.earscirev.2021.103517.

Agard, P., Handy, M., 2021. Ocean subduction dynamics in the Alps. Elements 17, 6–16. https://doi.org/10.2138/gselements.17.1.9.

Agard, P., Jolivet, L., Goffe, B., 2001. Tectonometamorphic evolution of the Schistes Lustrés complex: implications for the exhumation of HP and UHP rocks in the Western Alps. Bull. Soc. Geol. Fr. 172, 617–636. https://doi.org/10.2113/172.5.617.

Angel, R.J., Mazzucchelli, M.L., Alvaro, M., Nimis, P., Nestola, F., 2014. Geobarometry from host-inclusion systems: the role of elastic relaxation. Am. Mineral. 99 (10), 2146–2149. https://doi.org/10.2138/am-2014-5047.

Angel, R.J., Mazzucchelli, M., Alvaro, M., Nestola, F., 2017. EosFit-Pinc: a simple GUI for host-inclusion elastic thermobarometry. Am. Mineral. 102 (9), 1957–1960. https://doi.org/10.2138/am-2017-6190.

Angel, R.J., Murri, M., Mihailova, B., Alvaro, M., 2019. Stress, strain and Raman shifts. Z. Kristallogr. Cryst. Mater. 234 (2), 129–140. https://doi.org/10.1515/zkri-2018-2112.

Angel, R.J., Gilio, M., Mazzucchelli, M., Alvaro, M., 2022. Garnet EoS: a critical review and synthesis. Contrib. Mineral. Petrol. 177 (5), 54. https://doi.org/10.1007/s00410-022-01918-5.

Angiboust, S., Glodny, J., 2020. Exhumation of eclogitic ophiolitic nappes in the W. Alps: new age data and implications for crustal wedge dynamics. Lithos 356-357, 105374. https://doi.org/10.1016/j.lithos.2020.105374.

Angiboust, S., Agard, P., Jolivet, L., Beyssac, O., 2009. The Zermatt-Saas ophiolite: the largest (60-km wide) and deepest (c. 70–80km) continuous slice of oceanic lithosphere detached from a subduction zone? Terra Nova 21, 171–180. https://doi.org/10.1111/j.1365-3121.2009.00870.x.

Angiboust, S., Langdon, R., Agard, P., Waters, D., Chopin, C., 2012. Eclogitization of the Monviso ophiolite (W. Alps) and implications on subduction dynamics. J. Metamorph. Geol. 30, 37–61. https://doi.org/10.1111/j.1525-1314.2011.00951.x.

Balestro, G., Cadoppi, P., Perrone, G., Tallone, S., 2009. Tectonic evolution along the Col del Lis-Trana deformation zone (internal Western Alps). Boll. Soc. Geol. Ital. 128, 331–339.

Ballèvre, M., Camonin, A., Manzotti, P., Poujol, M., 2020. A step towards unravelling the paleogeographic attribution of pre-Mesozoic basement complexes in the Western Alps based on U-Pb geochronology of Permian magmatism. Swiss J. Geosci. 113, 12. https://doi.org/10.1186/s00015-020-00367-1.

Bearth, P., 1967. Die Ophiolithe der Zone von Zermatt-Saas Fee. In: Beiträge zur Geologischen Karte der Schweiz, Neue Folge, 132, p. 130.

Beltrando, M., Compagnoni, R., Lombardo, B., 2010. (Ultra-) high-pressure metamorphism and orogenesis: an alpine perspective. Gondwana Res. 18, 147–166. https://doi.org/10.1016/j.gr.2010.01.009.

Bose, K., Ganguly, J., 1995. Quartz-coesite transition revisited: reversed experimental determination at 500–1200 C and retrieved thermochemical properties. Am. Mineral. 80, 231–238.

Bousquet, R., Oberhänsli, R., Goffé, B., Wiederkehr, M., Koller, F., Schmid, S.M., Schuster, R., Engi, M., Berger, A., Martinotti, G., 2008. Metamorphism of metasediments in the scale of an orogen: a key to the tertiary geodynamic evolution of the Alps. In: Siegesmund, S., Fügenschuh, B., Froitzheim, N. (Eds.), Tectonic Aspects of the Alpine-Dinaride-Carpathian System, 298. Geological Society, London, Special Publications, pp. 393–412. https://doi.org/10.1144/SP298.18.

Boyer, H., Smith, D.C., Chopin, C., Lasnier, B., 1985. Raman microprobe (RMP) determinations of natural and synthetic coesite. Phys. Chem. Miner. 12, 45–48. https://doi.org/10.1007/BF00348746.

Brown, M., 2023. Some thoughts about eclogites and related rocks. Eur. J. Mineral. 35, 523–547. https://doi.org/10.5194/ejm-35-523-2023.

Bucher, K., Grapes, R., 2009. The eclogite-facies Allalin gabbro of the Zermatt-Saas ophiolite, Western Alps: a record of subduction zone hydration. J. Petrol. 50, 1405–1442.

Bucher, K., Fazis, Y., De Capitani, C., Grapes, R., 2005. Blueschists, eclogites, and decompression assemblages of the Zermatt–Saas ophiolite: high-pressure metamorphism of subducted Tethys lithosphere. Am. Mineral. 90, 821–835. https://doi.org/10.2138/am.2005.1718.

Campomenosi, N., Mazzucchelli, M.L., Mihailova, B., Scambelluri, M., Angel, R.J., Nestola, F., Reali, A., Alvaro, M., 2018. How geometry and anisotropy affect residual strain in host-inclusion systems: coupling experimental and numerical approaches. Am. Mineral. 103 (12), 2032–2035. https://doi.org/10.2138/am-2018-6700CCBY.

Campomenosi, N., Rubatto, D., Hermann, J., Mihailova, B., Scambelluri, M., Alvaro, M., 2020. Establishing a protocol for the selection of zircon inclusions in garnet for Raman thermobarometry. Am. Mineral. 105, 992–1001. https://doi.org/10.2138/am-2020-7246.

Campomenosi, N., Scambelluri, M., Angel, R.J., Hermann, J., Mazzucchelli, M.L., Mihailova, B., Piccoli, F., Alvaro, M., 2021. Using the elastic properties of zircon-garnet host-inclusion pairs for thermobarometry of the ultrahigh-pressure Dora-Maira whiteschists: problems and perspectives. Contrib. Mineral. Petrol. 176, 36. https://doi.org/10.1007/s00410-021-01793-6.

Campomenosi, N., Angel, R.J., Alvaro, M., Mihailova, B., 2023. Resetting of zircon inclusions in garnet: implications for elastic thermobarometry. Geology 51 (1), 23–27. https://doi.org/10.1130/G50431.1.

Carlson, W.D., 2006. Rates of Fe, Mg, Mn, and Ca diffusion in garnet. Am. Mineral. 91 (1), 1–11. https://doi.org/10.2138/am.2006.2043.

Chapman, T., Clarke, G.L., Daczko, N.R., 2019. The role of buoyancy in the fate of ultra-high-pressure eclogite. Sci. Rep. 9, 19925. https://doi.org/10.1038/s41598-019-56475-y.

Chopin, C., 1984. Coesite and pure pyrope in high-grade blueschists of the western Alps: a first record and some consequences. Contrib. Mineral. Petrol. 86, 107–118. https://doi.org/10.1007/BF00381838.

Chopin, C., 2003. Ultrahigh-pressure metamorphism: tracing continental crust into the mantle. Earth Planet. Sci. Lett. 212, 1–14. https://doi.org/10.1016/S0012-821X(03)00261-9.

Cloos, M., Shreve, R.L., 1988. Subduction-channel model of prism accretion, melange formation, sediment subduction, and subduction erosion at convergent plate margins: 1. Background and description. Pure Appl. Geophys. 128, 455–500. https://doi.org/10.1007/BF00874548.

Compagnoni, R., Rolfo, F., Carswell, D.A., Compagnoni, R., 2003. Ultrahigh-pressure units in the Western Alps in "ultrahigh-pressure metamorphism". In: EMU Notes in Mineralogy, vol. 5. Eötvös University Press, Budapest, pp. 13–49. https://doi.org/10.1180/EMU-notes.5.2.

Dal Piaz, G.V., Bistacchi, A., Massironi, M., 2003. Geological outline of the Alps. Episodes 26, 175–180.

De Togni, M., Gattiglio, M., Ghignone, S., Festa, A., 2021. Pre-alpine tectonostratigraphic reconstruction of the Jurassic Tethys in the high-pressure Internal Piedmont Zone (Stura di Viù Valley, Western Alps). Minerals 11, 361. https://doi.org/10.3390/min11040361.

De Togni, M., Gattiglio, M., Balestro, G., Roà, M., 2023. Alpine structural evolution of the Internal Piedmont Zone in the Upper Viù Valley (Lanzo Valleys Ophiolite, Western Alps). Rend. Online Soc. Geol. Ital. 60 https://doi.org/10.3301/ROL.2023.27.

Ehlers, A.M., Zaffiro, G., Angel, R.J., Boffa-Ballaran, T., Carpenter, M., Alvaro, M., Ross, N.L., 2022. Thermoelastic properties of zircon: implications for geothermobarometry. Am. Mineral. 107 (1), 74–81. https://doi.org/10.2138/am-2021-7731.

Frezzotti, M.L., Selverstone, J., Sharp, Z.D., Compagnoni, R., 2011. Carbonate dissolution during subduction revealed by diamond-bearing rocks from the Alps. Nat. Geosci. 4, 703–706. https://doi.org/10.1038/ngeo1246.

Frezzotti, M.-L., Huizenga, J.-M., Compagnoni, R., Selverstone, J., 2014. Diamond formation by carbon saturation in C–O–H fluids during cold subduction of oceanic lithosphere. Geochim. Cosmochim. Acta 143, 68–86. https://doi.org/10.1016/j.gca.2013.12.022.

Gasco, I., Gattiglio, M., Borghi, A., 2011. Lithostratigraphic setting and P-T metamorphic evolution for the Dora Maira Massif along the Piedmont Zone boundary (middle Susa Valley, NW Alps). Int. J. Earth Sci. 100, 1065–1085. https://doi.org/10.1007/s00531-011-0640-8.

Ghignone, S., Balestro, G., Gattiglio, M., Borghi, A., 2020a. Structural evolution along the Susa Shear Zone: the role of a first-order shear zone in the exhumation of meta-ophiolite units (Western Alps). Swiss J. Geosci. 113 (1), 1–16. https://doi.org/10.1186/s00015-020-00370-6.

Ghignone, S., Gattiglio, M., Balestro, G., Borghi, A., 2020b. Geology of the Susa Shear Zone (Susa Valley, Western Alps). J. Maps 16 (2), 79–86. https://doi.org/10.1080/17445647.2019.1698473.

Ghignone, S., Borghi, A., Balestro, G., Castelli, D., Gattiglio, M., Groppo, C., 2021a. HP-tectonometamorphic evolution of the Internal Piedmont Zone in Susa Valley (Western Alps): new petrologic insight from garnet+chloritoid –bearing micaschists and Fe-Ti metagabbro. J. Metamorph. Geol. 39 (4), 391–416. https://doi.org/10.1111/jmg.12574.

Ghignone, S., Sudo, M., Balestro, G., Borghi, A., Gattiglio, M., Ferrero, S., van Schijndel, V., 2021b. Timing of exhumation of meta-ophiolite units in the Western Alps: new tectonic implications from $^{40}Ar/^{39}Ar$ white mica ages from Piedmont Zone (Susa Valley). Lithos 404–405, 106443. https://doi.org/10.1016/j.lithos.2021.106443.

Ghignone, S., Scaramuzzo, E., Bruno, M., Livio, F., 2023a. A new UHP unit in the Western Alps: first occurrence of coesite from the Monviso Massif (Italy). Am. Mineral. 108 (7), 1368–1375. https://doi.org/10.2138/am-2022-8591.

Ghignone, S., Prencipe, M., Manzotti, P., Bruno, M., Boero, F., Borghini, A., Costa, E., Ciriotti, M., Scaramuzzo, E., 2023b. The Raman spectrum of florencite-(REE) [REEAl3(PO4)2(OH)6]: an integrated experimental and computational approach. J. Raman Spectrosc. 55 (3), 394–405. https://doi.org/10.1002/jrs.6640.

Gilio, M., Scambelluri, M., Agostini, S., Godard, M., Pettke, T., Agard, P., Locatelli, M., Angiboust, S., 2020. Fingerprinting and relocating tectonic slices along the plate interface: evidence from the Lago Superiore unit at Monviso (Western Alps). Lithos 352-353, 105308. https://doi.org/10.1016/j.lithos.2019.105308.

Gilio, M., van Schrojenstein Lantman, H.W., Girani, A., Angel, R.J., Scambelluri, M., Alvaro, M., 2022. The prograde history of three Mn-rich garnets from the UHP Lago di Cignana Unit (Italy). In: 15th Emile Argand Conference on Alpine Geological Studies, alpshop2022, p. 23.

Gilotti, J.A., 2013. The realm of ultrahigh-pressure metamorphism. Elements 9, 255–260. https://doi.org/10.2113/gselements.9.4.255.

Gouzu, C., Yagi, K., Thanh, N.X., Itaya, T., Compagnoni, R., 2016. White mica K–Ar geochronology of HP–UHP units in the Lago di Cignana area, western Alps, Italy: tectonic implications for exhumation. Lithos 248, 109–118. https://doi.org/10.1016/j.lithos.2016.01.015.

Groppo, C., Beltrando, M., Compagnoni, R., 2009. The P-T path of the ultra-high pressure Lago Di Cignana and adjoining high-pressure meta-ophiolitic units: insights into the evolution of the subducting Tethyan slab. J. Metamorph. Geol. 27, 207–231. https://doi.org/10.1111/j.1525-1314.2009.00814.x.

Groppo, C., Ferrando, S., Gilio, M., Botta, S., Nosenzo, F., Balestro, G., Festa, A., Rolfo, F., 2019. What's in the sandwich? New P–T constraints for the (U)HP nappe stack of southern Dora-Maira Massif (Western Alps). Eur. J. Mineral. 31 (4), 665–683. https://doi.org/10.1127/ejm/2019/0031-2860.

Kohn, M.J., 2020. A refined zirconium-in-rutile thermometer. Am. Mineral. 105, 963–971. https://doi.org/10.2138/am-2020-7091.

Kylander-Clark, A.R.C., Hacker, B.R., Mattinson, C.G., 2012. Size and exhumation rate of ultrahigh-pressure terranes linked to orogenic stage. Earth Planet. Sci. Lett. 321–322, 115–120. https://doi.org/10.1016/j.epsl.2011.12.036.

Lanari, P., Engi, M., 2017. 3. Local bulk composition effects on metamorphic mineral assemblages. In: Kohn, Matthew J., Engi, Martin, Lanari, Pierre (Eds.), Petrochronology: Methods and Applications, 2017. De Gruyter, Berlin, Boston, pp. 55–102. https://doi.org/10.1515/9783110561890-004.

Liou, J.G., Zhang, R., Liu, F., Zhang, Z., Ernst, W.G., 2012. Mineralogy, petrology, U-Pb geochronology, and geologic evolution of the Dabie-Sulu classic ultrahigh-pressure metamorphic terrane, East-Central China. Am. Mineral. 97 (10), 1533–1543. https://doi.org/10.2138/am.2012.4169.

Locatelli, M., Verlaguet, A., Agard, P., Federico, L., Angiboust, S., 2018. Intermediate-depth brecciation along the subduction plate interface (Monviso eclogite, W. Alps). Lithos 320–321, 378–402. https://doi.org/10.1016/j.lithos.2018.09.028.

Mancktelow, N.S., 1993. Tectonic overpressure in competent mafic layers and the development of isolated eclogites. J. Metamorph. Geol. 11, 801–812.

Manzotti, P., Schiavi, F., Nosenzo, F., Pitra, P., Ballèvre, M., 2022. A journey towards the forbidden zone: a new, cold, UHP unit in the Dora-Maira Massif (Western Alps). Contrib. Mineral. Petrol. 177, 59. https://doi.org/10.1007/s00410-022-01923-8.

Mazzucchelli, M.L., Burnley, P., Angel, R.J., Morganti, S., Domeneghetti, M.C., Nestola, F., Alvaro, M., 2018. Elastic geothermobarometry: corrections for the geometry of the host-inclusion system. Geology 46 (3), 231–234. https://doi.org/10.1130/G39807.1.

Mazzucchelli, M.L., Angel, R.J., Alvaro, M., 2021. EntraPT: an online platform for elastic geothermobarometry. Am. Mineral. 106 (5), 830–837. https://doi.org/10.2138/am-2021-7693CCBYNCND.

Mingardi, G., Campomenosi, N., Gilio, M., Chopin, C., Scambelluri, M., Alvaro, M., 2023. Elastic thermobarometry of ultrahigh-pressure metapelites from the Brossasco Isasca unit (Dora-Maira Massif, Western Alps). Lithos. https://doi.org/10.1016/j.lithos.2023.107167.

Murri, M., Mazzucchelli, M.L., Campomenosi, N., Korsakov, A.V., Prencipe, M., Mihailova, B., Scambelluri, M., Angel, R.J., Alvaro, M., 2018. Raman elastic geobarometry for anisotropic mineral inclusions. Am. Mineral. 103 (11), 1869–1872. https://doi.org/10.2138/am-2018-6625CCBY.

Özkan, H., Cartz, L., Jamieson, J.C., 1974. Elastic constants of nonmetamict zirconium silicate. J. Appl. Phys. 45 (2), 556–562. https://doi.org/10.1063/1.1663283.

Reinecke, T., 1991. Very-high-pressure metamorphism and uplift of coesite-bearing metasediments from the Zermatt-Saas zone, Western Alps. Eur. J. Mineral. 3, 7–17. https://doi.org/10.1127/ejm/3/1/0007.

Rubatto, D., Hermann, J., 2003. Zircon formation during fluid circulation in eclogites (Monviso, Western Alps): implications for Zr and Hf budget in subduction zones. Geochim. Cosmochim. Acta 67, 2173–2187. https://doi.org/10.1016/S0016-7037(02)01321-2.

Rubatto, D., Gebauer, D., Fanning, M., 1998. Jurassic formation and Eocene subduction of the Zermatt-Saas-fee ophiolites; implications for the geodynamic evolution of the Central and Western Alps. Contrib. Mineral. Petrol. 132, 269–287. https://doi.org/10.1007/s004100050421.

Rubatto, D., Burger, M., Lanari, P., Hattendorf, B., Schwarz, G., Neff, C., Schmidt, P.K., Hermann, J., Vho, A., Gunter, D., 2020. Identification of growth mechanisms in metamorphic garnet by high-resolution trace element mapping with LA-ICP-TOFMS. Contrib. Mineral. Petrol. 175, 61. https://doi.org/10.1007/s00410-020-01700-5.

Schmid, S.M., Kissling, E., Diehl, T., van Hinsbergen, D.J.J., Molli, G., 2017. Ivrea mantle wedge, arc of the Western Alps, and kinematic evolution of the Alps–Apennines orogenic system. Swiss J. Geosci. 110, 581–612. https://doi.org/10.1007/s00015-016-0237-0.

Schönig, J., von Eynatten, H., Meinhold, G., Keno, N., Lünsdorf, K., 2022. The sedimentary record of ultrahigh-pressure metamorphism: a perspective review. Earth-Sci. Rev. 227, 103985 https://doi.org/10.1016/j.earscirev.2022.103985.

Skora, S., Mahlen, N.J., Johnson, C.M., Baumgartner, L.P., Lapen, T.J., Beard, B.L., Szilvagyi, E.T., 2015. Evidence for protracted prograde metamorphism followed by rapid exhumation of the Zermatt-Saas fee ophiolite. J. Metamorph. Geol. 33, 711–734.

Smith, D.C., 1984. Coesite in clinopyroxene in the Caledonides and its implications for geodynamics. Nature 310, 641–644.

Sobolev, N.V., Shatsky, V.S., 1990. Diamond inclusions in garnets from metamorphic rocks: a new environment for diamond formation. Nature 343, 742–746.

Stangarone, C., Angel, R.J., Prencipe, M., Campomenosi, N., Mihailova, B., Alvaro, M., 2019. Measurement of strains in zircon inclusions by Raman spectroscopy. Eur. J. Mineral. 31 (4), 685–694. https://doi.org/10.1127/ejm/2019/0031-2851.

Taguchi, T., Kouketsu, Y., Igami, Y., Kobayashi, T., Miyake, A., 2021. Hidden intact coesite in deeply subducted rocks. Earth Planet. Sci. Lett. 558, 116763 https://doi.org/10.1016/j.epsl.2021.116763.

Tajčmanová, L., Manzotti, P., Alvaro, M., 2021. Under pressure: high-pressure metamorphism in the Alps. Elements 17 (1), 17–22. https://doi.org/10.2138/gselements.17.1.17.

von Roermund, H.L.M., Carswell, D.A., Drury, M.R., Heijboer, T.C., 2002. Microdiamonds in a megacrystic garnet websterite pod from Bardane on the island of Fjørtoft, western Norway: evidence for diamond formation in mantle rocks during deep continental subduction. Geology 30 (11), 959–962. https://doi.org/10.1130/0091-7613(2002)030<0959:MIAMGW>2.0.CO;2.

Wang, J., Mao, Z., Jiang, F., Duffy, T.S., 2015. Elasticity of single-crystal quartz to 10 GPa. Phys. Chem. Miner. 42, 203–212.

Warr, L.N., 2021. IMA–CNMNC approved mineral symbols. Mineral. Mag. 85, 291–320. https://doi.org/10.1180/mgm.2021.43.

Weber, S., Bucher, K., 2015. An eclogite-bearing continental tectonic slice in the Zermatt–Saas high-pressure ophiolites at Trockener Steg (Zermatt, Swiss Western Alps). Lithos 232, 336–359.

Xiong, J.W., Chen, Y.X., Zhou, K., Schertl, H.P., Zheng, Y.F., Huang, F., Xia, X.-P., Chen, Z.W., 2021. Fe and O isotopes in coesite-bearing jadeite quartzite from the Western Alps record multistage fluid-rock interactions in a continental subduction zone. Geochim. Cosmochim. Acta 312, 1–24. https://doi.org/10.1016/j.gca.2021.08.006.

Zanoni, D., Rebay, G., Spalla, M.I., 2016. Ocean floor and subduction record in the Zermatt-Saas rodingites, Valtournanche, Western Alps. J. Metamorph. Geol. 34, 941–961. https://doi.org/10.1111/jmg.12215.

Zhang, L., Ellis, D.J., Jiang, W., 2002. Ultrahigh-pressure metamorphism in western Tianshan, China: part I. Evidence from inclusions of coesite pseudomorphs in garnet and from quartz exsolution lamellae in omphacite in eclogites. Am. Mineral. 87, 853–860.